The influence of self-assembled monolayers on the practical adhesion of a cataphoretic paint

Agathe Rougier [a], Maëlenn Aufray [b*], Jean-Marie Melot [a], Francis Touyeras [a], Xavier Roizard [c], Xavier Gabrion [c], Jean-Yves Hihn [a], Fabrice Lallemand [a].

[a] *Université de Franche-Comté, Laboratoire UTINAM UMR 6213 CNRS, IUT Besançon-Vesoul Département Chimie, 30 avenue de l'Observatoire - BP 1559, 25009 BESANCON Cedex, France*

[b] *CIRIMAT, Université de Toulouse, CNRS, INP-ENSIACET, 4 allée Émile Monso, BP 44362, 31030 Toulouse cedex 4, France*

[c] *Université de Franche-Comté, FEMTO ST UMR 6174 CNRS, Département de mécanique appliquée, 24 chemin de l'épitaphe, 25000 BESANCON, France*

** corresponding author: maelenn.aufray@ensiacet.fr*

Agathe Rougier, rougier.agathe@gmail.com

NO ORCID

Maëlenn Aufray, maelenn.aufray@ensiacet.fr*

ORCID: 0000-0001-5921-6322

Jean-Marie Melot, jean-marie.melot@univ-fcomte.fr

ORCID: 0000-0001-6483-4467

Francis Touyeras, francis.touyeras@univ-fcomte.fr

NO ORCID

Xavier Roizard, xavier.roizard@univ-fcomte.fr

ORCID: 0000-0002-3115-1835

Xavier Gabrion, xavier.gabrion@femto-st.fr

ORCID: 0000-0002-2796-6361

Fabrice Lallemand, fabrice.lallemand@univ-fcomte.fr

ORCID: 0000-0003-1898-8670

Jean-Yves Hihn, jean-yves.hihn@univ-fcomte.fr

ORCID: 0000-0002-7857-2098

Word count: 9790 words

ABSTRACT

The objective of this study is to replace steel-phosphating treatments with self-assembled monolayers (SAMs), in this case, of phosphonic acids. Two industrial applications are targeted:

- Obtaining an adhesion primer between steel and paint or lubricating stainless steel for mechanical applications, such as stamping.
- Research has been conducted using alkyl phosphonic acids. The carbon chain length and terminal function are changed to obtain the best properties depending on the application.

Keywords: Self-assembled monolayers, adhesion, primer, stainless steel

I. Introduction

Since the 1990s, regulations relating to knowledge of chemicals and assessment of their risks have led industries to innovate and develop increasingly environmentally friendly products. The steel-phosphating process, initiated in 1907 with the Coslett patent [1], is a surface treatment with several disadvantages: the production of metallic waste necessitates several rinses with subsequent treatments over time, requiring staff to follow these treatments. The presence of nitrites, nitrates, and concentrated acids in the bath requires hazardous manipulations [2]. Moreover, the miniaturization of currently manufactured products to achieve a thickness of approximately 10 to 30 µm is also problematic. A phosphatation replacement should ensure anti-corrosion, adhesion to paint, and anti-wear properties.

Thus, in recent years, research has been conducted on alternatives to phosphate coatings. Different options are currently available on the market or described in the literature. These include phosphating with a modified composition [3], sol-gels [4-20], and very thin coatings such as self-assembled monolayers (SAMs).

As phosphating is used for not only its adhesion and anti-corrosion properties but also its anti-wear properties, alternatives exist for applications such as cold forming and lubrication. In recent years, research has been conducted on dry lubricants to solve the problems of waste and cleaning after lubrication, which are costly for industries. These dry lubricants are manufactured with self-assembled monolayers. This nanometer-scale deposition is obtained by immersing a metal substrate in a modification solution containing active molecules at a low concentration [21-22]. These molecules are grafted onto the surface oxides by chemisorption [23], forming a monolayer with different properties depending on the molecules used. Since the early 2000s, SAMs have been increasingly used for their ease of manipulation, reproducibility, stability [24], and versatility [25]. Research has focused on alkylphosphonic acids to continue using an environmentally friendly process [26-29]. Notably, studies performed on copper showed improved tribological [30] and anti-corrosion properties [31-32]. A few years later, a new process for surface functionalization without surface preparation was patented and applied in industry [33].

Research has been conducted using phosphonic acids to obtain adherence properties on copper with a carboxylic termination [34-35]. This study was conducted based on this research. In this research, practical adhesion (*i.e.* adherence) was studied with two adherence tests: the single lap joint (SLJ) (AFNOR, NF EN 2243-1) and three-point bending (AFNOR, ISO 14679: 1997) tests. An epoxy-based glue, Araldite 103-1, with a hardener, HY 991, was used to closely align with the industrial conditions of cataphoretic painting, which also has an epoxy function. Phosphate coating is replaced with SAMs, where the carbon chain length and the terminal

function have been modified to obtain the best properties from the phosphating treatment and the best fracture resistance.

II. Materials and methods

1. Material and sample preparation

a. *Substrates*

The metallic substrate used was a plate of austenitic AISI 304 stainless steel (304SS) with a thickness of 0.8 mm for three-point bending tests. The 304SS substrate had a thickness of 0.5 ± 0.05 mm for the SLJ and pull-off test. The chemical composition and roughness parameters are shown in Table 1.

b. *Synthesis of alkylphosphonic acids*

All alkylphosphonic acids were synthesized in the laboratory. All molecules are represented in Figure 1 and were analyzed by ^{1}H and ^{31}P Nuclear magnetic resonance *(*NMR). Their purity exceeded 95%.

Other syntheses are described (see below).

<u>11-phosphonoundecanoic acid (C10COOH) synthesis</u>:

Although commercially available, this product can be efficiently synthesized in multigram quantities from cheap materials. Commercial 11-bromoundecanoic acid from Sigma Aldrich was esterified with excess absolute ethanol in the presence of 96% sulphuric acid for 24 h. After cooling, the solution was neutralized with solid sodium hydrogen carbonate and concentrated *in vacuo*. The residue was dissolved in ether/water. The ethereal phase was washed with saturated sodium hydrogen carbonate and dried. Evaporation of the solvent afforded ethyl 11-bromoundecanoate, which was sufficiently pure for the following steps. The previous ester was

heated to 190°C and excess triethylphosphite (1.75–2.0 equivalents) added dropwise by stirring. Bromoethane was continuously distilled as formed (35°C–40°C/760 mm Hg). The temperature was raised to 210°C–215°C until no more bromoethane was extracted. A vacuum (20–50 mm Hg) was progressively established with caution: excess triethylphosphite was distilled with an undesirable contaminant (diethyl ethylphosphonate). The mixture, containing mainly the triethyl ester of 11-phosphonoundecanoic acid, was cooled to room temperature; 12 M aqueous hydrochloric acid was added and the mixture gently boiled with efficient stirring for 24 h (85°C–90°C). On cooling to room temperature by stirring, crude 11-phosphonoundecanoic acid was separated into thick plates, filtered, and washed with water. Recrystallization from acetic acid afforded pure 11-phosphonoundecanoic acid as a white powder or off-white needles. The overall yield was 75% with a melting point of 175°C–177°C.

1,12-dodecanediphosphonic acid (-C12 (2P)-) synthesis:

According to the work of S. Frey *and al.* [61], diethyl 1,12-dodecanediphosphonate was synthesized from 1,12-dibromododecane (Alfa Aesar) and a sixfold molar excess of triethylphosphite (Alfa Aesar) at 200°C before being hydrolyzed by refluxing from concentrated 12 M aqueous HCl for 24 h. The thick diacid, which precipitated readily in the reaction mixture, was filtered, washed free of strong acid with distilled water, and dried in air. It was purified by recrystallization from an acetic acid/DMSO mixture. The overall yield obtained was 65% with a melting point of 175°C–179°C.

10-undecenylphosphonic acid (C9CH=CH2) synthesis:

Bromoethane was formed by distilling, while 11-bromo-undec-1-ene (Sigma Aldrich) mixed with a threefold molar excess of triethylphosphite (Alfa Aesar) was heated to 200°C. After the reaction, excess phosphite and diethyl ethylphosphonate was distilled off (P = 40–50 mm Hg), leaving diethyl undecenylphosphonate as an oil in almost quantitative yield; 15 g of the

preceding phosphonate was dissolved in 70 mL of dichloromethane and cooled in an ice bath, while 20 mL of bromotrimethylsilane was added in four portions. No exothermic phenomena were observed. After standing at 0°C for 30 min, the reaction was left at room temperature overnight. Evaporation of the solvent produced a relatively mobile oil. Methanol (100 mL) and water (5 mL) were then added and the mixture left for 24 h. After evaporation of the solvent, the oily residue crystallized in ice. It was then recrystallized from heptane to give slightly gray needles. The overall yield obtained is 41% with a melting point of 80°C–84°C.

1,5-phosphonopentadecanoic acid (C14COOH) synthesis:

The 1,5-bromoundecanoic acid was prepared from pentadecanolide (Sigma Aldrich) in a 90% yield according to [61]; 15-phosphonopentadecanoic acid was then obtained as a white powder, following method A. The melting point obtained was 118°C–121°C.

Previous research has described the syntheses of several alkylphosphonic acids, such as butanephosphonic acid (C4P) [36], dodecanephosphonic acid (C12P) [32], and hexadecanephosphonic acid (C16P) [36].

c. *Surface preparation*

Pretreatment of samples

The 304SS was immersed by stirring in an alkaline degreasing bath (Presol 7060, Coventya, France) for 2 min at 60°C. The substrate was then rinsed with distilled water and 96% ethanol. The 304SS was sonicated in 96% ethanol for 10 min before being rinsed with 96% ethanol and distilled water. Finally, samples were dried with pressurized air.

Grafting preparation

The substrate was immersed in an alkylphosphonic acid ethanolic modification solution for 8 h to ensure the most reproducible results with good organization of SAMs on the surface (Table 2) [36-37]. In some cases, it was then rinsed with 96% ethanol and distilled water. Finally, all the samples were dried in an oven for 30 min at 30°C.

d. *Glue and bonding thermal curing*

Grafted samples were adhesively bonded by applying a mixture of an epoxy prepolymer and an amine curing agent. The epoxy prepolymer is Araldite 103-1, while the hardener is HY 991 (Huntsman, USA). After bonding, samples were kept at room temperature for 3 hours. They were then heated in an oven for 1 hour at 150°C before cooling to room temperature for 1 hour.

2. Adherence tests

Adherence measurements were conducted with the SLJ and the three-point bending tests. SLJ results are usually reported as tension (MPa), while three-point bending test results are reported as force (N). In this document, all results are expressed as stress.

Single lap joint test (AFNOR, NF EN 2243-1)

The SLJ is a test designed for the initiation and propagation of fractures. The 304SS bare specimens used as substrates were milled for reuse after each test. First, a two-step surface preparation was conducted, followed by a surface modification treatment. In a second step, the specimens were placed in a special set-up allowing two substrates to be aligned, with the same adhesive joints. A syringe was used to apply 0.06 mL glue. A 3 kg weight was added to the specimens to ensure intimate contact between the surface and adhesive. The adhesive joint then complied with the bonding protocol indicated above. A series of five adhesive joints was prepared and tested for each configuration.

The tests were conducted on an MTS (USA) Criterion 45 machine with a 100 kN load cell at room temperature. The crosshead displacement speed was 1 mm/min. Specimen dimensions are described in Figure 2 (left). The maximum force (F_{max}) was considered as the load at breaking point, while the ultimate load was divided by the overlap to evaluate the lap shear strength (σ_{max} in MPa).

b. *Three-point bending test (AFNOR, ISO 14679: 1997)*

Plates of 304SS were used to perform the three-point bending test. First, the plates complied with the surface preparation protocol before undergoing surface modifications. In a second step, Araldite 103-1 with hardener HY991 was applied to the cut (10.0 ± 0.1 mm × 50.0 ± 0.1 mm). Specimens of 304SS were prepared by applying 0.5 mL with a syringe in a silicone mold between two clamping plates to form an adhesive block 25 × 5 × 4 mm^3. A series of eight samples was prepared and tested for each configuration.

These tests were conducted at room temperature (23 ± 2°C) with a tensile machine (INSTRON 3369, USA) equipped with a 500 N full-scale load cell with a sensitivity of 0.5%. The displacement rate was 0.500 ± 0.003 mm/min in the three-point configuration (Figure 2 [right]). The distance between supports was 35 mm (the norm indicating a space of 33 mm). The ultimate load, F_{max}, was considered as the failure initiation measurement [38]. The bending stress was calculated by dividing the load by the adhesive surface area.

c. *Aging with the Bac Ford test (ISO 2812-2:2007)*

The Bac Ford test is used to analyze the aging and corrosion of automotive paintwork. It comprises a tank where samples are immersed in demineralized water at 40°C with an angle of 15–20° for several days [34]. Our specimens are produced as described above with the addition of a 24 µm film of glue to the surface to match real conditions as closely as possible. The

immersion time was set at 3 days.

3. Surface characterization

Treated surfaces were characterized by microstructural and chemical analysis using different surface analytical techniques.

a. *Surface energy*

Surface energy measurements were conducted using the drop shape analyzer (DSA25) from Krüss (Germany) in drop mode. The apparatus was equipped with a camera to perform automatic measurements.

Several solvents were chosen to use the Owens, Wendt, Rabel, and Kaelble (OWRK) [40] calculation method (Equations 1–2 and Table 3).

$$\sigma_{sl} = \sigma_s + \sigma_l - 2\left(\sqrt{\sigma_s^d \times \sigma_l^d} + \sqrt{\sigma_s^p \times \sigma_l^p}\right) \qquad \text{(Equation 1)}$$

σ_{sl}: Interfacial tension between liquid and solid phases

σ_s: Interfacial tension of solid phase

σ_l: Interfacial tension of liquid phase

σ_s^d: Dispersive component of solid phase

σ_l^d: Dispersive component of liquid phase

σ_s^p: Polar component of solid phase

σ_l^p: Polar component of liquid phase

Θ: Contact angle at triple point

$$\sigma_{sl} = \sigma_s - \sigma_l \times cos\theta \qquad \text{(Equation 2)}$$

A σ_l versus $\frac{\sigma_l^p}{\sqrt{\sigma_l^d}}$ curve was plotted to obtain the surface energy of the test specimen using drop angles derived from the solvents used. Surface energies were obtained with a determination coefficient R^2 exceeding 0.9.

Ideally, an apolar solvent should also be used; however, measurements with heptane and cyclohexane are difficult due to low wettability angles.

Eight angle measurements were taken for the same drop. The contact angle measurement was conducted by considering both angles of the drop on the substrate surface. The time interval between points was 1.5 s, and each solvent was tested with four drops.

Therefore, it was possible to view the drops and measurements taken directly on the associated Advance software. Surface energy calculations of the samples were obtained by the software.

b. *Friction test*

An Anton Paar circular tribometer was used to conduct a tribological study of different grafts on the steel surface. After theoretical calculations based on the Hertz contact theory, a 5 mm diameter 100Cr6 ball was used as a friction pin with a normal load of 1 N. Thus, the theoretical mean pressure under contact was P_{mean} = 440 MPa. Before testing, the ball was cleaned with ethanol and dried. The test speed was set at v = 1 rnd.s^{-1} (leading to linear velocities of 12 to 20 mm.s^{-1} according to the friction track radius); 30 cycles were performed, and each test was conducted at least three times.

c. *Microstructure analysis*

Field emission scanning electron microscopy with energy dispersive X-ray spectroscopy

(FESEM/EDX) was used to study the morphological surface using a Tescan Mira3 (Czech Republic) instrument. Roughness was measured using an Infinite Focus optical microscope from Alicona Imaging GmbH (France). X-ray photoelectron spectroscopy (XPS) was used to measure the elemental composition to determine the surface compositions of the three-point bending samples after testing. Spectra were acquired using monochromatized Al Kα radiation (1486.6 eV), and analyses were conducted at a photoelectron angle of 45°. The X-ray radiation source operated in a vacuum of 3×10^{-9} mbar. The binding energies of core levels were calibrated as a function of the C1s binding energy set at 284.8 eV, a characteristic energy of alkyl moieties. Deconvolutions were performed using mixed Gaussian–Lorentzian curves (80% Gaussian character) with CasaXPS software.

d. *Polarization modulation infrared reflection adsorption spectroscopy (PM-IRRAS)*

PM-IRRAS orientation measurements were used to probe the orientation of bonds associated with IR excitation of specific molecular vibrational modes. A Bruker Vertex 70 (USA) IR spectrometer was used. The samples were positioned to obtain the largest signal amplitude; 36 scans were performed for each sample, and the resolution was 4 cm^{-1}. The detector was positioned at an angle of 75°, according to results by F. Roy [36]. After acquisition, the spectra were processed with the OPUS software. C-H vibration bands of CH_3 (wave numbers: ν_s = 2875 cm^{-1}, ν_a = 2964 cm^{-1}) and CH_2 (ν_s = 2851 cm^{-1}, ν_a = 2921 cm^{-1}) were analyzed to determine how the SAMs were organized on the substrate surface [36].

e. *Glass transition temperature determination*

Differential scanning calorimetry (DSC) experiments were performed in a Mettler (DSC 1, Switzerland) apparatus to determine the glass transition temperature (T_g) of Araldite with various surface modifications. Aluminum pans containing a few mg of polymer were heated

from −10°C to 180°C at a heating rate of 10°C.min^{-1} under a continuous flow of oxygen and argon in the first step. (This cycle is not considered in the study because two effects remain possible: the end of the glue cross-linking and the removal of water from the sample.) After a temperature drop, a second pass from -10°C to 180°C with a heating rate of 20°C/min was performed to get a better visualization of the glass transition event. Only the last step is presented in this paper. The T_g was determined from the onset point (corresponding to the beginning of the glass transition) for coatings from various treatments.

III. Results

Two sets of tests were conducted. The first focused on the impact of SAMs on 304SS specimens. The second compared the two treatment processes: the classical one with phosphate coated steel and the alternative process with stainless steel modified with SAMs.

The 304SS surface modification with SAMs can be used as an early grip layer before classical cataphoretic painting. Several SAMs were tested, in which the terminal function, carbon chain length, or both were modified. A glue with the same epoxy base as this paint was used to ensure a simpler study system.

The adherence study was conducted using two adherence tests, the SLJ and three-point bending. Measurements were characterized before the test by PM-IRRAS and surface energy. A study of metal/polymer interactions was also conducted by DSC with the glass transitions to understand the phenomena observed during the adherence tests.

1. Adherence test

a. *Other parameters affecting adherence: post-modification rinsing*

Rinsed samples have better resistance to failure (21.5 ± 1.8 MPa) than unrinsed samples (4.8 ± 1.8 MPa). Rinsing samples after surface modification removes species from solution together with physisorbed clusters that form a weak attachment to the substrate (Figure 3). This layer leads to poor adherence, though it is beneficial for obtaining the tribological properties [32; 41].

b. *Impact of carbon chain length*

Three SAMs of 4, 12, and 16 carbons were examined. Treatments were tested with the SLJ and the three-point bending test. Results are expressed as stress (MPa) to compare the adherence of SAMs in two failure modes (modes II and I).

Figure 4 shows the three-point bending and SLJ results for these three SAMs. The same order of magnitude was observed for the SAMs/epoxy system and the 304SS/epoxy reference. The stress involved is approximately 15 times greater in mode II (SLJ) stress than in mode I (three-point bending). In the latter case, we divided by the adhesive surface area: $S = 5 \times 25 = 125$ mm². In reality, the fracture is initiated on a much smaller surface (Figure 5). The restitution of elastic energy during three-point bending is transferred to the interface and participates in the propagation of the fracture. Therefore, crack propagation is virtually independent of the adhesive surface [42].

These tests cannot be compared in terms of values obtained as stresses vary. The results obtained for the different treatment conditions are compared in each case.

In the three-point bending test, adding SAMs significantly improves the bending strength. Without SAMs, the maximum bending stress is approximately 0.06 MPa, whereas

after adding SAMs, the maximum bending stress is between 1.0 and 1.1 MPa. Furthermore, the carbon chain length does not appear to impact the bending stress.

In SLJ, adding SAMs with apolar endings to the surface of 304SS decreases the shear stress, except for C12P, which does not alter the shear stress limit.

In the SLJ test, observing the test pieces may indicate mixed adhesive and cohesive fracture modes, contrary to three-point bending samples (Figure 6). In the three-point bending test, tear-offs are completely adhesive between the SAMs and epoxy polymer. In our case, no fracture initiation on the three-point bending specimens was observed. SAMs are transparent and too thin to be observed under a microscope. To quickly and easily check the sample fracture location, we have developed an original test measuring the friction coefficient. Indeed, friction coefficients are very different for steel (304SS), a polymer (Araldite), and a SAM. Thus, the type of fracture can be ascertained by determining the friction coefficients on the surfaces of the test specimens:

♦ Adhesive: both surfaces have different coefficients.

♦ Cohesive: both surfaces have the same friction coefficient.

Friction coefficients were measured at the point of adhesive failure on the test specimens after the adherence test using an Anton Paar circular tribometer [43]. These test results are shown in Figure 7. For the 304SS (reference without SAMs), the friction coefficient is around 0.5 after 30 cycles. For all SAMs except C4P, we found a friction coefficient below 0.2 after 30 cycles, which is typical of the friction coefficient of a polymer such as Araldite glue for these load conditions (see Figure 8). For the C4P treatment, differences exist in the friction coefficient, which is closer to stainless steel than for the other SAMs tested.

Measurements were performed on the epoxy adhesive deposited on a 304SS specimen to verify

the friction coefficient. Different thicknesses of epoxy adhesive were deposited to observe what adhesive film remained on the three-point bending specimens. Figure 8 shows the friction coefficients obtained for specimens with an epoxy adhesive on surface films with thicknesses of 24, 60, and 100 μm. These measurements were performed at least three times each.

According to Figure 8, the friction coefficient of the epoxy adhesive is below that observed on the three-point bending test specimens. Furthermore, we were surprised to observe a slight decrease in the friction coefficient as the adhesive film thickness decreased. Therefore, the friction coefficient cannot be correlated with the film thickness remaining on the surfaces of the three-point bending test specimens.

Based on these results, the fracture appears to be adhesive to the interphase SAM/adhesive for C4P. For all the other SAMs, the friction coefficients are between 0.08 and 0.18, indicating either an adhesive failure between the SAM and the adhesive or a cohesive failure in the adhesive. Therefore, an XPS analysis of the specimen interface was conducted to verify these results by another method.

The surface was characterized before testing to understand the interface present at the time of bonding. Figure 9 represents the surface energy of SAMs with a chain length of 4 to 16 carbons. Surface energies were obtained using the OWRK method [40] with three solvents (water, ethylene glycol, and glycerol). Alkaline degreasing followed by ultrasonic degreasing in ethanol was conducted to preserve the surface oxides and hydroxides [44]. Surface oxides create a strong bond by chemisorption when SAMs are grafted to the surface. Moreover, we observed that C4P has a higher surface energy than C12P. When the carbon chain length is small, a slight overlap exists in the plate surface. Therefore, the substrate is visible, accounting for the relatively high uncertainties for C4P. Indeed, C4P has a poor distribution on the surface of the specimens [36], confirming the friction coefficients (intermediate between stainless steel and

SAMs). Observation of total surface energy indicates that the higher the carbon number in the alkyl chain, the lower the total surface energy. However, the dispersive component of surface energy has the same tendency as the three-point bending adherence results. Therefore, it appears that the adherence achieved by adding SAMs is related to the dispersive energy of the interface under test.

In the remainder of this study, C12P was retained, as this molecule provides good adherence in the three-point bending test without altering shear adherence. The impact of the terminal function was then tested with four different terminations: two apolar (alkyl and alkene) and two polar (carboxylic and phosphonic acid).

c. *Impact of terminal groups*

The effect of the terminal function was tested using a chain length of 11–12 carbons with polar (carboxylic and phosphonic acid) and apolar (alkyl and alkene) functions. Figure 10 compares the maximum stresses at the fracture point for shear and three-point bending where the terminal function was modified.

In SLJ, the terminal function has no impact, except for C9-CH=CH2, where a slight increase in shear stress is observed. In the three-point bending test, an improvement in bending stress is observed for polar endings such as carboxylic and phosphonic acid functions. The polar endings may therefore create interactions with the adhesive. Moreover, these two chemical functions can react with one another by forming dimers for carboxyl functions, while phosphonic acid groups can form bridges between them.

A friction test was conducted under the same conditions as before to verify that fracture occurs in the SAM (see Figure 11).

According to Figure 11, adding SAMs allows a decrease in the friction coefficient approaching

0.2. Based on the above observations, this friction coefficient is obtained from the presence of an epoxy adhesive film remaining on the surface of the specimens after the three-point bending test. Except for C4P (Figure 7), failure of the three-point bending test specimen dots appears cohesive in the adhesive.

XPS analysis of the chemical compositions of sample surfaces after three-point bending was conducted to validate these hypotheses (Table 4).

The chemical composition presented in Table 4 shows an absence of phosphorus for C10COOH and C12(2P) specimens. Furthermore, these specimens contain the same chemical species as the epoxy adhesive, with approximately the same proportions of each element. The iron present in the substrate is detected in very small quantities. This information indicates that, on the three-point bending test specimens, failure is therefore cohesive in the epoxy adhesive. For C4P, a low proportion of phosphorus exists, as well as the same chemical elements as the epoxy adhesive, with an iron content higher than in C10COOH and C12(2P). This confirms that C4P has an adhesive failure at the interphase of the SAMs and the adhesive, as elements of both the adhesive and the SAMs are present in the failure zone. Evidence also exists that C4P is not evenly distributed over the substrate surface due to the relatively high iron content.

These observations show that specimens with a friction coefficient of approximately 0.2 exhibit cohesive failure in the adhesive in the three-point bending tests. For C4P, the friction coefficient is between 0.2 (values for other SAMs) and 0.4 (values for the 304SS reference). This is consistent with the chemical composition of the tested interface, indicating that the fracture is adhesive in the SAM/adhesive interphase.

A surface energy study was then conducted on these two SAMs, as illustrated in Figure 12. This showed a decrease in the total surface energy when treated with SAMs, compared to reference 304SS (without surface treatment on the specimen). Moreover, the decrease in the total surface

energy and polar component was lower when a polar carboxylic function was added. This indicates that the terminal function is perpendicular to the surface.

Figures 10 and 12 demonstrate the impact of surface modification by SAMs. Therefore, the latter improves adherence, especially with a chain length of 11 carbons with a carboxyl polar terminal group, providing an adherence primer.

For Figures 4 and 10, we demonstrated that the termination of SAMs is more important than the carbon chain length in obtaining a high maximum stress. Nothdurft showed that for two polar carboxylic- terminated molecules, the best peel adherence results on copper were obtained for C15COOH (16-phosphonohexadecanoic acid) compared to C5COOH (6-phosphonohexanoic acid) [35]. Therefore, the question arose regarding whether a longer carbon chain length in the presence of a carboxyl termination could improve the adherence of our system.

Figure 13 compares bending stresses for C12P and C16P with those for C10COOH and C14COOH, respectively. The results are compared to the reference without surface modification with the 304SS.

As shown above, the carbon chain length with an apolar alkyl termination does not impact three-point bending adherence. According to Figure 13, for a longer carbon chain with a polar (carboxyl) termination, a decrease in bending stress is observed (for C14COOH compared to C10COOH). Therefore, the carbon chain length plays a major role in polar terminations. A decrease in adherence for C14COOH may originate from good SAM organization of long carbon chains and the creation of hydrogen bonds between them, forming dimers [35].

d. *Comparison with reference coating: Phosphating process*

This study aims to replace the phosphate coating. The results were previously compared to the

reference system (Figure 14). On the left, the reference system comprises a zinc-phosphate coating on low alloy steel. On the right, the replacement system comprises 304SS to improve the anti-corrosion properties where SAMs are grafted on its surface.

A calculation was conducted to eliminate the substrates to compare these two systems and the adherence results obtained in three-point bending tests. This calculation was performed to obtain the adherence energy to compare both systems.

Figure 15 shows a standard three-point bending curve. The diagrams of the bonded assemblies show each test stage up to the initiation of specimen failure. Force "Fa" represents the force required to break the bonded assembly, while force "Fs" corresponds to the force required to initiate the bending of the substrate only. To break the bonding joint, the deflection distance *d* is required (measured by tensile machine). The following calculation obtains the energy required to break the bonded assembly by separation from the substrate.

According to the publication by Alain Roche [45], the adherence energy is deduced from Equation 3, which includes all the energies of specimen components. All these energies are calculated for the same deflection, $d = d_{failure}$, for each tested specimen.

$$E_{adherence} = E_{tot} - E_{substrate} \qquad \text{(Equation 1)}$$

E_{tot}: total energy of the specimen
$E_{substrat}$: elastic deformation energy of the substrate

This calculation is used to formulate Equations 4 and 5, determining the adherence energy (E_a) according to the treatment used by freeing the substrate.

$$E_{adherence} = \frac{(F_a \times d)}{2} - \frac{(F_s \times d)}{2} \qquad \text{(Equation 2)}$$

$$E_{adherence} = \frac{(F_a - F_s)d}{2} \qquad \text{(Equation 5)}$$

The results of the different tests were processed using equation 5 (figure 16). The results show an improvement in adherence between modified 304SS and phosphating. The Adherence energy increases when SAMs are grafted onto the surface. For an apolar alkyl-type termination, the adherence energy increases with the carbon chain length.

For C12P and C9-CH=CH2, the adherence energies are essentially the same. This result is relatively consistent as the carbon chain length is similar, and the terminal function is apolar in both cases. However, the standard deviation obtained is smaller. This may be due to the presence of the double bond, which gives greater stability to the bonded assembly through stabilizing π-π interactions, a privileged conformation, or both. Indeed, the rigidity of the termination, which prevents its rotation in the assembly, leads to greater entanglement of the molecules with one another and the adhesive.

In C10COOH, adding a carboxyl polar group allows a significant increase in adherence energy compared to C12P (alkyl terminal function). This increase is probably because the carboxyl termination reacts with the adhesive and forms dimers that stiffen the bonded assembly. This observation applies to C12(2P), which also has a polar termination yielding a higher bond energy than C12P. In this molecule, the polar phosphonic termination can react with the adhesive but also form bridges on the substrate surface or create bonds between them. These possibilities lead to rigidity of the bonded assembly with an inter-entanglement of molecules longer than C12P.

An aging study of the three-point bending test specimens was conducted using the Bac Ford test to identify the cumulative effect of SAMs in relation to the current phosphating system.

e. *Aging of samples using the Bac Ford test*

A Bac Ford wet aging test was conducted for 3 days to place the specimens in more aggressive conditions to reduce the adherence energies. Figure 17 shows the impact of 3-day aging in the Bac Ford test in terms of adherence energy to compare these results with phosphating (reference system). The results show that the coating from phosphating treatment is only slightly affected by this wet aging, whereas, except for the C9-CH=CH2 molecule, all other systems are more heavily impacted.

C4P shows a slight decrease in adherence energy after aging for 3 days. We observed that the longer the carbon chain length, the greater the impact of aging on the bonded assembly, resulting in a sharp decrease in the system adherence energy. Evidently, the performance of SAMs comprising molecules with a long carbon chain is significantly impacted by wet aging.

The coating containing the C10COOH molecules is seriously damaged by this aging, which may be due to an acid-base reaction (by dissociation) occurring at the carboxylic acid termination [pKa_1(COOH) = 4.5–5]. The results for C12(2P) are identical, as a significant decrease in adherence energy is observed. This phenomenon must be due, first, to an acid-base reaction of the terminal function of phosphonic acid [Pka1(phosphonic) = 2–3] and, second, to bond formation between terminations resulting in greater chain spacing, allowing incorporation of water molecules into the thin film.

Contrary to these two coatings, the one comprising the C9-CH=CH2 termination did not react to this aging. The entanglement of these molecules, described above, and the apolar terminal function make the coating visibly less accessible to water. A characterization study of interfaces and grafting was conducted to verify the various hypotheses presented in this paper.

2. *Surface and interface characterization*

a. *SAM organization*

The various surface SAMs were observed by PM-IRRAS. CH_3 and CH_2 vibration bands were analyzed to understand the organization of SAMs on the substrate surface. Indeed, CH_3 and CH_2 vibrations of SAMs are characteristic when well-organized.

Symmetrical (s) and asymmetrical (a) vibration frequencies of the methylene group (CH_2) systematically tend towards $\nu_s(CH_2) = 2850\ cm^{-1}$ and $\nu_a(CH_2) = 2920\ cm^{-1}$, according to Spori *et al.* [41]. Frequency variation is known to be sensitive to the conformational order of alkyl chains, shifting to higher frequencies with a conformational disorder. Symmetrical and asymmetrical vibration frequencies of the methyl group (CH_3) tend towards $\nu_s(CH_3) = 2870\ cm^{-1}$ and $\nu_a(CH_3) = 2960\ cm^{-1}$, while their positions remain almost invariable depending on the chain conformation according to Spori *et al.* [46].

The observed values of CH_3 vibration bands are almost constant, of the order of 2960 cm^{-1}, with minimal variation depending on the SAMs tested. The length of the carbon chain influenced the locations of the CH_2 vibration bands, especially the symmetrical one. Indeed, the vibration frequency appears at 2859 cm^{-1} for short chains such as C4P, a high value being characteristic of a disordered alkyl chain [46]. For chain lengths exceeding 12 atoms (C14COOH, C16P, and C20P), vibration bands appear at 2850 cm^{-1}, indicating that these molecules adopt a crystalline, well-organized structure. For intermediate chains with a length of 11–12 carbons, the sym-band is located at a value between 2850 and 2860 cm^{-1}, indicating a semi-crystalline structure [C10COOH: $\nu_s(CH_2) = 2854\ cm^{-1}$; C12P: $\nu s(CH_2) = 2860\ cm^{-1}$].

Several research teams observed these phenomena and concluded that short carbon chains of SAMs are disordered, whereas long carbon chains (C > 11–12) produce well-organized structures on the surface of the substrate [36] [46-55]. For intermediate chain lengths, a mixed

organization is observed with a semi-crystalline system.

b. *Study of metal/polymer interaction: glass transitions*

DSC was conducted using a Mettler instrument (DSC 1) to determine the T_g of Araldite in contact with the various SAMs. When in contact with the SAMs, the epoxy network changed, leading to a difference in T_g [56-58].

The difference in T_g may be due to the following:

- Stiffness of SAMs,
- Molecular mass of SAMs,
- Decrease in free volume between SAMs and epoxy,
- Decreased mobility of SAMs with increased reticulation,

or a combination of the above conditions [59].

The adhesive undergoes the same curing cycle as in the adherence tests. Therefore, it must have the same T_g regardless of the surface treatment.

Measurements of the T_g of the glue/substrate interphase with varying glue thicknesses were compared to values obtained by the glue in its volume (Figure 18). These measurements indicated that the T_g of the interphase is higher at lower glue thicknesses, leading to stable mechanical properties in a larger temperature range. In this study, an optimum value was obtained for a 24 µm glue thickness. Subsequently, the remainder of this study was conducted with 24 µm films for comparison with samples used for adherence to simulate a glue joint "towards the glue/SAM interface" (Figure 19).

An optimum T_g of 96 ± 1°C was obtained for C12(2P). C12(2P) can form bridges on the substrate surface through phosphonic acid functions. Building network rigidity leads to reduced

mobility of SAMs and accounts for the greater T_g.

PM-IRRAS measurements showed a mixed organization for a chain length of 11–12 carbons, which favors an increase in the layer density of SAMs, as for C12P. SAMs have a similar T_g to 304SS.

IV. Discussion and visualization of SAM organization

1. Results overview

The analyses and tests showed an improvement in adherence after adding SAMs, depending on SAMs organization. Let us know that the SAMs organization is directly linked to their composition (carbon chain length and terminal function). Table 5 provides an overview of these results.

2. Visualization of SAM organization

The various adherence tests and the characterization study of surfaces in terms of surface energy, PM-IRRAS, DSC, and XPS allow us to propose an organization model of the different SAMs tested (Table 6).

Short-chain molecules (C4P) do not completely cover the substrate surface. Previous studies show that C4P is not correctly organized on the surface [36]. The molecules become entangled and agglomerate.

Long-chain SAMs (C16P) allow Van der Waals interactions, permitting orientated organization of molecules in relation to one another. In terms of adherence, this good organization of apolar

terminations does not ensure good adherence with the epoxy, which was also observed with carboxylic terminations (C14COOH).

For SAMs of average carbon chain length [C12P, C9-CH=CH2, C10COOH, and C12(2P)], PM-IRRAS and XPS are inadequate with chain entanglement, as well as with the presence of organized molecules. This combination of both types of configuration results in superior adherence compared to other chain lengths.

Such a combination of organizations in the presence of a polar termination (carboxylic and phosphonic acid) results in an adherence primer capable of surpassing phosphatization regarding three-point bending stresses.

This modeling confirms several studies with a short chain length. SAMs do not organize themselves or completely cover the substrate surface [46; 60]. With a chain length exceeding 14 carbons, SAMs are organized automatically through London interactions. An intermediate chain length allows a good overlap due to mixed organization [36]. Moreover, adding a polar termination allows the creation of new interactions between molecules of the Keesom and Debye type, which will generate good cohesion of the bonded assembly.

V. Conclusions

In this study, alkylphosphonic acids were investigated to replace steel-phosphating treatments. Before the modification treatment, 304SS substrates were immersed in an alkaline degreasing bath. After modification with alkylphosphonic acids, we confirmed that it is essential to conduct optimized rinsing to remove physisorbed clusters from the surface to obtain a good-quality thin film with better adherence.

This research studied practical adhesion with two adherence tests: the SLJ and three-point bending tests. To simulate the industrial conditions of cataphoretic painting, we used an epoxy-

based glue, Araldite 103-1, with a hardener, HY 991, which also has an epoxy function. Phosphating treatment is replaced with SAMs where the carbon chain length and the terminal function have been modified. According to the three-point bending tests, confirmed by friction coefficient measurements at the break site, fractures are cohesive in the adhesive, except for C4P, where the fracture is adhesive in the SAM/adhesive interphase. The shear test results show that SAMs comprising molecules with short or long carbon chain lengths lead to decreased adherence compared to 304SS. The results for a median chain length (C12P) are comparable to the substrate. Terminations do not appear to impact the maximum shear stress, whereas a slight improvement could be observed with C9-CH=CH2.

In three-point bending, adding SAMs improves adherence. A carbon chain with an apolar termination minimally impacts the maximum shear stress. A polar termination with a length of 11–12 carbons has been shown to improve adherence. In both tests, grafting with alkylphosphonic acids appears to be optimized with a chain length of 11–12 carbons.

The surface energy is consistent with the adherence results and allows modeling of the organization of the different SAMs. A chain length of 11–12 carbons gives a semi-crystalline organization of SAMs.

Adherence energy results enabled the comparison of the two systems studied: phosphate coating on steel and SAMs grafted on stainless steel. It appears that treatment with SAMs significantly improves system adherence. Nevertheless, the replacement system is more sensitive to wet aging than the phosphate coating, except for C9-CH=CH2, which shows higher adherence after aging.

In three-point bending, a terminal polar function of a carboxylic or phosphonic acid type allows a good adherence primer to be obtained.

Finally, the optimal condition for better adhesion is a mixture of ordered and entangled SAMs. Reducing the grafting time to 30 seconds could allow this configuration to be obtained, making the treatment compatible with industrial conditions.

Acknowledgment

The authors wish to thank Aurélien Buteri from APERAM Inc. for the supply of 304SS; Nicolas Rouge for SEM images; Vincent Tissot for machining of installations for bonded assembly samples, as well as for shear bites; and Olivier Heintz for XPS analysis.

Declaration of interest statement

The authors declare that they have no known competing financial interests or personal relationships that could have appeared to influence the work reported in this paper.

References

[1] Thomas Watts Coslett. Treatment of iron or steel for preventing oxidation or rusting. November 12 1907. US Patent 870,937.

[2] TSN Sankara Narayanan. Surface pretretament by phosphate conversion coatings-a review. *Reviews in Advanced Materials Science*, 9:130–177, 2005.

[3] Feng Fang, Jing-hua Jiang, Shu-Yong Tan, Ai-bin Ma, and Jian-qing Jiang. Characteristics of a fast low-temperature zinc phosphating coating accelerated by an eco-friendly hydroxylamine sulfate. *Surface and Coatings Technology*, 204(15):2381–2385, 2010.

[4] I Milošev and GS Frankel. Conversion coatings based on zirconium and/or titanium. *Journal of The Electrochemical Society*, 165(3):C127–C144, 2018.

[5] L Fedrizzi, FJ Rodriguez, S Rossi, F Deflorian, and R Di Maggio. The use of electrochemical techniques to study the corrosion behaviour of organic coatings on steel

pretreated with sol–gel zirconia films. *Electrochimica Acta*, 46(24-25):3715–3724, 2001.

[6] Masahiko Matsukawa, Kazuhiro Makino, and Toshiaki Shimakura. Chemical conversion coating agent and surface-treated metal, December 23 2004. US Patent 2004,018,7967.

[7] Donald R Vonk, Edis Kapic, Bruce Goodreau, and Alvaro Bobadilla. Metal pretreatment composition containing zirconium, copper, zinc, and nitrate and related coatings on metal substrates, June 25 2012. US Patent 2012,030,1739.

[8] Donald R Vonk, Edis Kapic, and Michael L Sienkowski. Metal pretreatment composition containing zirconium, copper, and metal chelating agents and related coatings on metal substrates, March 12 2013. US Patent 2013,026,6819.

[9] HR Asemani, P Ahmadi, AA Sarabi, and H Eivaz Mohammadloo. Effect of zirconium conversion coating: Adhesion and anti-corrosion properties of epoxy organic coating containing zinc aluminum polyphosphate (zapp) pigment on carbon mild steel. *Progress in Organic Coatings*, 94:18–27, 2016.

[10] Hossein Eivaz Mohammadloo, Ali Asghar Sarabi, Ali Asghar Sabbagh Alvani, Hassan Sameie, and Reza Salimi. Nano-ceramic hexafluorozirconic acid based conversion thin film: Surface characterization and electrochemical study. *Surface and Coatings Technology*, 206(19-20):4132–4139, 2012.

[11] Patrick Droniou, William E Fristad, and Jeng-Li Liang. Nanoceramic-based conversion coating: Ecological and economic benefits position process as a viable alternative to phosphating systems. *Metal finishing*, 103(12):41–43, 2005.

[12] VONK Donald, Edis Kapic, Bruce Goodreau, and Alvaro Bobadilla. Metal pretreatment composition containing zirconium, copper, zinc and nitrate and related coatings on metal substrates, August 23 2018. US Patent App. 15/961,262.

[13] Nguyen Van Chi, Pham Trung San, To Thi Xuan Hang, Truong Anh Khoa, Nguyen Hoang, Nguyen Thu Hien, et al. Corrosion protection of carbon steel using zirconium oxide/silane pretreatment and powder coating. *Vietnam Journal of Science and Technology*, 57(1):38, 2019.

[14] WJ Van Ooij, Danqing Zhu, M Stacy, A Seth, T Mugada, J Gandhi, and P Puomi. Corrosion protection properties of organofunctional silanes An overview. *Tsinghua Science and technology*, 10(6):639–664, 2005.

[15] B Ramezanzadeh, E Raeisi, and M Mahdavian. Studying various mixtures of 3-aminopropyltriethoxysilane (aps) and tetraethylorthosilicate (teos) silanes on the

corrosion resistance of mild steel and adhesion properties of epoxy coating. *International Journal of Adhesion and Adhesives*, 63:166–176, 2015.

[16] Cecilia Deyá. Silane as adhesion promoter in damaged areas. *Progress in Organic Coatings*, 90:28–33, 2016.

[17] C Motte, M Poelman, A Roobroeck, M Fedel, F Deflorian, and M-G Olivier. Improvement of corrosion protection offered to galvanized steel by incorporation of lanthanide modified nanoclays in silane layer. *Progress in Organic Coatings*, 74(2):326–333, 2012.

[18] Vera Rosa Capelossi and Idalina Vieira Aoki. Influence of sonication on anticorrosion properties of a sulfursilane film dopped with ce (iv) on galvannealed steel. *Progress in Organic Coatings*, 76(5):812–820, 2013.

[19] Juliana S Francisco, Vera Rosa Capelossi, and Idalina Vieira Aoki. Evaluation of a sulfursilane anticorrosive pretreatment on galvannealed steel compared to phosphate under a waterborne epoxy coating. *Electrochimica Acta*, 124:128–136, 2014.

[20] MGS Ferreira, RG Duarte, MF Montemor, and AMP Simoes. Silanes and rare earth salts as chromate replacers for pre-treatments on galvanised steel. *Electrochimica acta*, 49(17-18):2927–2935, 2004.

[21] Abraham Ulman. Formation and structure of self-assembled monolayers. *Chemical reviews*, 96(4):1533–1554, 1996.

[22] Frank Schreiber. Structure and growth of self-assembling monolayers. *Progress in surface science*, 65(5-8):151–257, 2000.

[23] Sidharam P Pujari, Luc Scheres, Antonius TM Marcelis, and Han Zuilhof. Covalent surface modification of oxide surfaces. *Angewandte Chemie International Edition*, 53(25):6322–6356, 2014.

[24] CR Kaufmann, G Mani, D Marton, DM Johnson, and CM Agrawal. Long-term stability of self-assembled monolayers on 316l stainless steel. *Biomedical Materials*, 5(2):025008, 2010.

[25] John G Van Alsten. Self-assembled monolayers on engineering metals: structure, derivatization, and utility. *Langmuir*, 15(22):7605–7614, 1999.

[26] Clémence Queffélec, Marc Petit, Pascal Janvier, D Andrew Knight, and Bruno Bujoli. Surface modification using phosphonic acids and esters. *Chemical reviews*, 112(7):3777–3807, 2012.

[27] Seid Yimer Abate, Ding-Chi Huang, Yu-Tai Tao, Surface modification of TiO2 layer with phosphonic acid monolayer in perovskite solar cells: Effect of chain length and terminal functional group, *Organic Electronics*, 78:105583, 2019

[28] Gaëlle Anne Léonie Andreatta, Nicolas Blondiaux, Antonin Faes, Spray coating vs. immersion for self-assembly of gemini perfluorinated phosphonic acids on indium tin oxide, *Thin Solid Films*, 732: 138783, 2021

[29] Dajana Mikić, Helena Otmačić Ćurković, Saman Hosseinpour, Bronze corrosion protection by long-chain phosphonic acids, *Corrosion Science*, 205: 110445, 2022

[30] Mohamed Moustapha Moine, Xavier Roizard, Jean-Marie Melot, Luc Carpentier, Pierre-Henri Cornuault, Fabrice Lallemand, Jean-Marie Rauch, Olivier Heintz, and Séverine Lallemand. Grafting and characterization of dodecylphosphonic acid on copper: Macro-tribological behavior and surface properties. *Surface and Coatings technology*, 232:567–574, 2013.

[31] Durainatarajan, Periyasamy; Prabakaran, Mallaiah; Ramesh, Subbaratnam, Self-assembled monolayers of novel imidazole derivative on copper surface for anticorrosion protection in neutral medium, *Journal of Adhesion Science & Technology*, 35(23): 2580-2601, 2021

[32] Hrimla, Meryem; Bahsis, Lahoucine; Boutouil, Aziz; Laamari, My Rachid; Julve, Miguel, A combined computational and experimental study on the mild steel corrosion inhibition in hydrochloric acid by new multifunctional phosphonic acid containing 1,2,3-triazoles , J*ournal of Adhesion Science & Technology*, 34(16): 1741-1773, 2020

[33] Fabrice Lallemand, Xavier Roizard, Jean-marie Melot, Aurélien Buteri, Mélanie Borgeot, and Romain Evrard. Surface treatment of metal substrates, February 5 2019. US Patent 10,196,744.

[34] Evelin Jaehne, Sonia Oberoi, and Hans-Juergen P Adler. Ultra thin layers as new concepts for corrosion inhibition and adhesion promotion. *Progress in Organic Coatings*, 61(2-4):211–223, 2008.

[35] Philipp Nothdurft, Sonja Feldbacher, Georg Jakopic, Inge Mühlbacher, Sandra Pötz, and Wolfgang Kern. Surface characterization of copper substrates modified with carboxyl terminated phosphonic acids. *International Journal of Adhesion and Adhesives*, 84:143–152, 2018.

[36] Florian Roy, Abdeslam Et Taouil, Fabrice Lallemand, Jean-Marie Melot, Xavier Roizard, Olivier Heintz, Virginie Moutarlier, and Jean-Yves Hihn. Influence of modification time and high frequency ultrasound irradiation on self-assembling of alkylphosphonic acids on stainless steel: Electrochemical and spectroscopic studies. *Ultrasonics sonochemistry*, 28:269–275, 2016.

[37] Daniel Garcia-Raya, Rafael Madueo, José Manuel Sevilla, Manuel Blizquez, and Teresa Pineda. Electrochemical characterization of a 1,8-octanedithiol self-assembled monolayer (odt-sam) on a au(111) single crystal electrode. *Electrochimica Acta*, 53(27):8026 – 8033, 2008.

[38] Sébastien Genty, Jean-Baptiste Sauvage, Philippe Tingaut, and Maëlenn Aufray. Experimental and statistical study of three adherence tests for an epoxy-amine/aluminum alloy system: Pull-off, single lap joint and three-point bending tests. *International Journal of Adhesion and Adhesives*, 79:50–58, 2017.

[39] Evelyne DARQUE-CERETTI and Bernard MONASSE. Mise en peinture des plastiques. *Techniques de l'ingénieur Finitions des plastiques, conceptions des pièces et recyclage*, base documentaire: TIB475DUO.(ref. article: am3785), 2010. fre.

[40] Daniel K Owens and RC Wendt. Estimation of the surface free energy of polymers. *Journal of applied polymer science*, 13(8):1741–1747, 1969.

[41] Pierre-Henri Cornuault, Jean-Marie Melot, Xavier Roizard, and Fabrice Lallemand. Dry lubrication of ferritic stainless steel functionalised with crystalline aggregates of hexadecylphosphonic acid. *Tribology International*, 145:106139, 2020.

[42] Jean-Baptiste Sauvage. *Caractérisation et modélisation de l'adhérence dans les assemblages collés*. PhD thesis, Mulhouse, 2016.

[43] Xavier Roizard, Jannica Heinrichs, Aurélien Butéri, Staffan Jacobson, Mélanie Borgeot, Luc Carpentier, Jean-Marie Melot, and Fabrice Lallemand. Friction behavior of ferritic stainless steel in a strongly diluted alcohol solution of alkylphosphonic acid. *Tribology International*, 118:465–473, 2018.

[44] M Mantel and JP Wightman. Influence of the surface chemistry on the wettability of stainless steel. *Surface and Interface analysis*, 21(9):595–605, 1994.

[45] A Roche, F Gaillard, M Romand, and M Von Fahnestock. Metal-adhesive bonded systems: Adhesion measurement using a three point flexure test. *Journal of Adhesion Science and Technology*, 1(1):145–157, 1987.

[46] Doris M Spori, Nagaiyanallur V Venkataraman, Samuele GP Tosatti, Firat Durmaz, Nicholas D Spencer, and Stefan Zürcher. Influence of alkyl chain length on phosphate self-assembled monolayers. *Langmuir*, 23(15):8053–8060, 2007.

[47] Peter Thissen, Markus Valtiner, and Guido Grundmeier. Stability of phosphonic acid self-assembled monolayers on amorphous and single-crystalline aluminum oxide surfaces in aqueous solution. *Langmuir*, 26(1):156–164, 2010.

[48] Nolan Tillman, Abraham Ulman, Jay S Schildkraut, and Thomas L Penner. Incorporation of phenoxy groups in self-assembled monolayers of trichlorosilane derivatives. Effects on film thickness, wettability, and molecular orientation. *Journal of the American Chemical Society*, 110(18):6136–6144, 1988.

[49] Rosalynn Quinones and Ellen S Gawalt. Study of the formation of self-assembled monolayers on nitinol. *Langmuir*, 23(20):10123–10130, 2007.

[50] Houston Byrd, John K Pike, and Daniel R Talham. Inorganic monolayers formed at an organic template: a langmuir-blodgett route to monolayer and multilayer films of zirconium octadecylphosphonate. *Chemistry of materials*, 5(5):709–715, 1993.

[51] Ralph G Nuzzo, Lawrence H Dubois, and David L Allara. Fundamental studies of microscopic wetting on organic surfaces. 1. Formation and structural characterization of a self-consistent series of polyfunctional organic monolayers. *Journal of the American Chemical Society*, 112(2):558–569, 1990.

[52] Marc D Porter, Thomas B Bright, David L Allara, and Christopher ED Chidsey. Spontaneously organized molecular assemblies. 4. Structural characterization of n-alkyl thiol monolayers on gold by optical ellipsometry, infrared spectroscopy, and electrochemistry. *Journal of the American Chemical Society*, 109(12):3559–3568, 1987.

[53] Michael Maxisch, Christoph Ebbert, Boray Torun, Nicole Fink, Teresa De Los Arcos, J Lackmann, Hans Jürgen Maier, and Guido Grundmeier. Pm-irras studies of the adsorption and stability of organophosphonate monolayers on passivated niti surfaces. *Applied Surface Science*, 257(6), 2011.

[54] Ch Bram, Ch Jung, and M Stratmann. Self assembled molecular monolayers on oxidized inhomogeneous aluminum surfaces. *Fresenius' journal of analytical chemistry*, 358(1-2):108–111, 1997.

[55] Zineb Mekhalif, Gregory Fonder, Fabrice Laffineur, and Joseph Delhalle. Comparative assessment of n-dodecanethiol and n-dodecaneselenol monolayers on electroplated copper. *Journal of Electroanalytical Chemistry*, 621(2):245–253, 2008.

[56] Hamid Bourahla, Jeanine Lenoir, Maurice Romand, and Jean Chauchard. Influence de l'épaisseur de l'adhésif et du vieillissement sur les propriétés mécaniques dynamiques d'un assemblage: adhésif structural/acier inoxydable. *Die Angewandte Makromolekulare Chemie: Applied Macromolecular Chemistry and Physics*, 178(1):47–62, 1990.

[57] AA Roche, J Bouchet, and S Bentadjine. Formation of epoxy-diamine/metal interphases. *International Journal of adhesion and Adhesives*, 22(6):431–441, 2002.

[58] J Bouchet and A.A. Roche. The formation of epoxy/metal interphases: mechanisms and their role in practical adhesion. *The Journal of Adhesion*, 78(9):799–830, 2002.

[59] Ch Oudet. Polymers structure and properties introduction; polymeres structure et proprietes introduction. 1993.

[60] Colin D Bain and George M Whitesides. Modeling organic surfaces with self-assembled monolayers. *Angewandte Chemie*, 101(4):522–528, 1989.

[61] S Frey, A Shaporenko, M Zharnikov, P Harder, and DL Allara. Self-assembled monolayers of nitrile-functionalized alkanethiols on gold and silver substrates. *The Journal of Physical Chemistry B*, 107(31):7716–7725, 2003.

Table 1: Chemical composition and roughness parameters of samples

	Fe	Cr	Ni	Sa (arithmetic mean height)	Sq (root mean square height)	Ssk (Skewness)	Sku (Kurtosis)
304 SS plate	72.93 %	18.47 %	8.60 %	4.49 µm	5.89 µm	0.08	4.44
304 SS bare	72.80 %	18.54 %	8.66 %	5.91 µm	7.45 µm	0.08	3.12

Table 2: Different SAMs

Molecules names	
Butanephosphonic acid	C4P
Dodecanephosphonic acid	C12P
Hexadecanephosphonic acid	C16P
11-phosphonoundecanoic acid	C10COOH
Dodecane-1,12-diphosphonic acid	C12(2P)
10-undecanephosphonic acid	C9CH=CH2
15-phosphonopentadecanoic acid	C14COOH

Table 3: Solvents interfacial tensions

Solvents	Interfacial tension σ_l (mJ/m²)	Dispersive component σ_l^d (mJ/m²)	Polar component σ_l^p (mJ/m²)
water	72.8	21.8	51
ethylene glycol	48.3	29.3	19
glycerol	63.4	37	26.4

Table 4: Analysis of sample composition by XPS in atomic percent (measurement uncertainties of 0.1 %)

	C1s	N1s	O1s	Si2p	P2p	Fe2p
C10COOH	68.1	2.6	21.0	8.0	-	0.2
C12(2P)	68.9	2.6	19.7	8.5	-	0.2
C4P	43.7	3.2	40.4	7.2	0.8	4.7
Epoxy adhesive	71.2	2.5	18.2	8.1		

Table 5: Results overview

Samples	Tensile stress test (MPa)	Three-Point bending test (MPa)	Surface energy (mN/m)	Dispersive part (mN/m)	Polar part (mN/m)	Adherence energy (mJ)		Glass transition (°C)	ν_s (CH_2) (cm^{-1})
						Without ageing	Ageing		
304SS (Reference)	20.3 ± 0.9	0.60 ± 0.07	50.67 ± 2.42	3.84 ± 0.56	46.82 ± 1.86	7.4 ± 2.9	0.6 ± 0.7	89 ± 1	
Phosphatation						3.5 ± 0.9	2.4 ± 1.2		
Reference values									2850
C4P	16.2 ± 1.4	1.03 ± 0.20	28.34 ± 30.35	10.19 ± 12.58	18.14 ± 2	21.4 ± 25.7	14.6 ± 4.2	88 ± 1	2859
C10COOH	20.7 ± 2.1	1.62 ± 0.15	33.8 ± 3.05	10.91 ± 1.3	22.89 ± 1.76	97.7 ± 30.7	2.7 ± 0.5	89 ± 1	2854
C12P	20.7 ± 1.0	0.93 ± 0.40	22.10 ± 4.34	9.94 ± 2.34	12.15 ± 2	29.8 ± 30.1	12.7 ± 6.9	92 ± 1	2860
C14COOH		0.21 ± 0.02							2849
C16P	13.7 ± 2.7	1.08 ± 0.10	21.05 ± 1.1	15.57 ± 0.74	5.47 ± 0.36	42.6 ± 7.8	0.3 ± 3.9	89 ± 1	2850
C9-CH=CH2	23.1 ± 2.6	1.02 ± 0.20				29.0 ± 17.1	34.6 ± 7.7	87 ± 1	
C12(2P)	17.6 ± 0.9	1.48 ± 0.14				74.4 ± 21.9	2.6 ± 2.3	96 ± 1	

Table 6: Modelling organisation of SAMs

C4P	C12P / C10COOH / C12(2P) / C9-CH=CH2	C16P / C14COOH / C20P
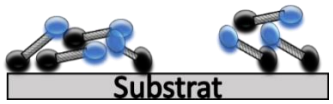	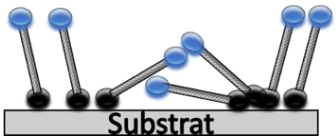	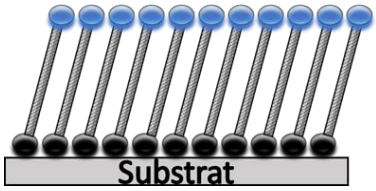

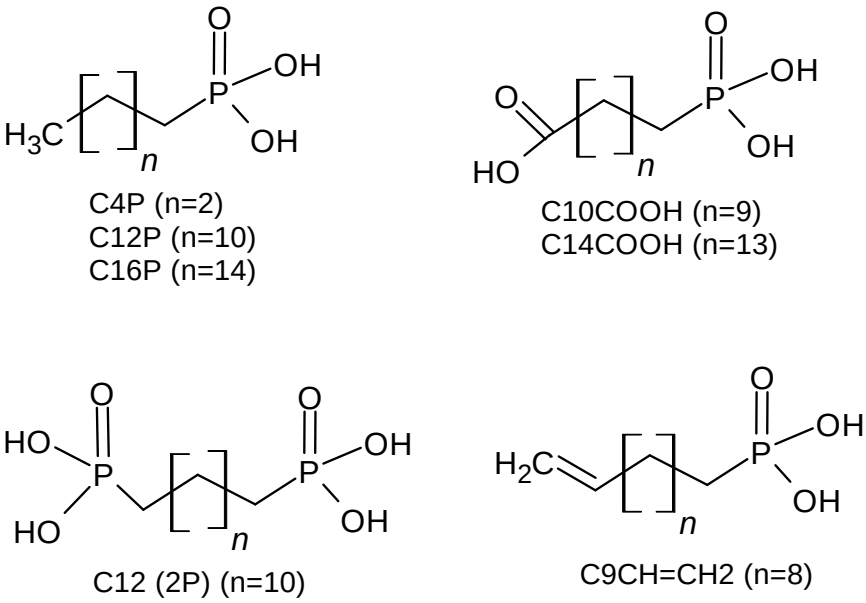

Figure 1: Different alkylphosphonic acids

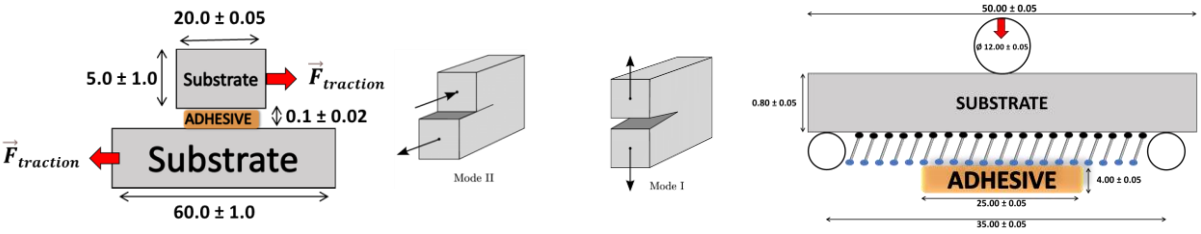

Figure 2: Single Lap Joint geometry, (not to scale, dimensions in mm) mode II solicitation (Left) and Three-point bending geometry (not to scale, dimensions in mm), mode I and II solicitation (Right)

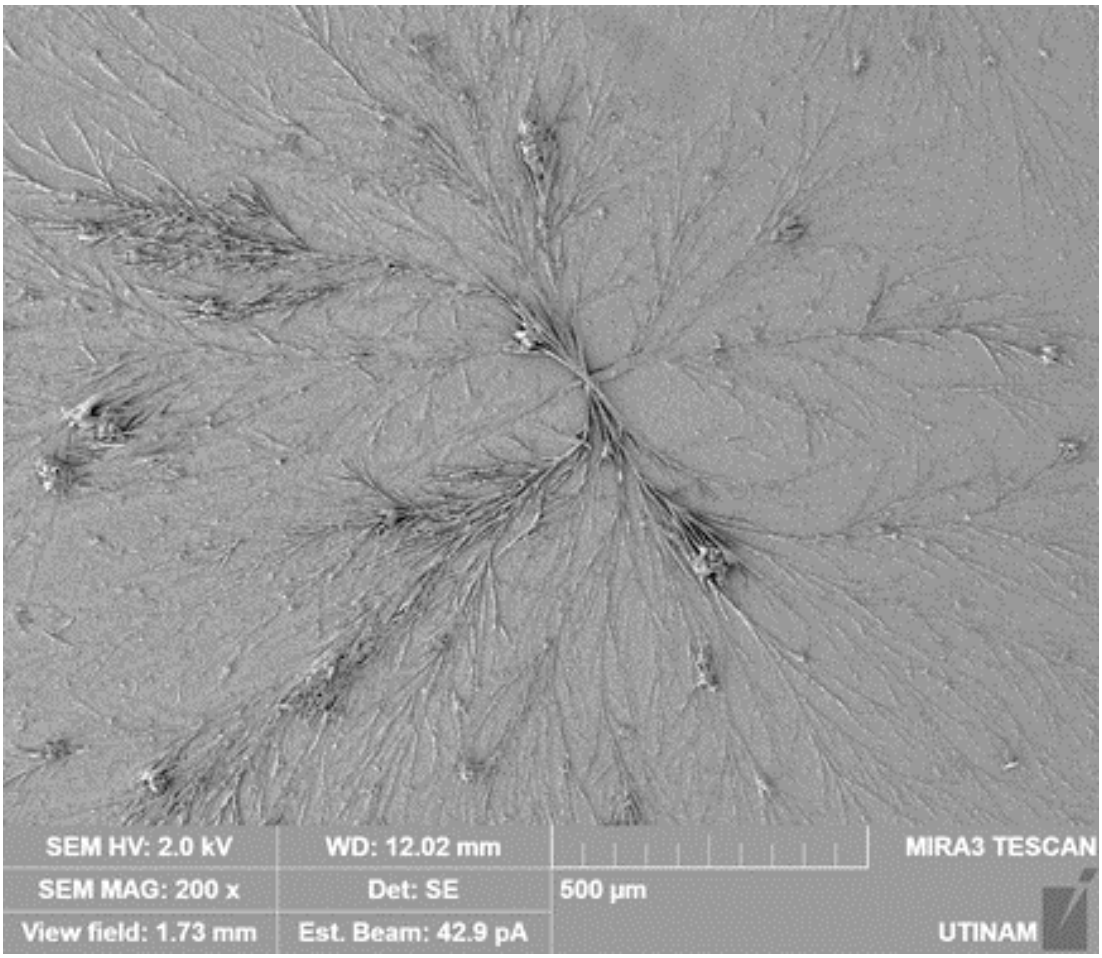

Figure 3: SEM picture of a physisorbed cluster on the surface sample without rinsing post modification

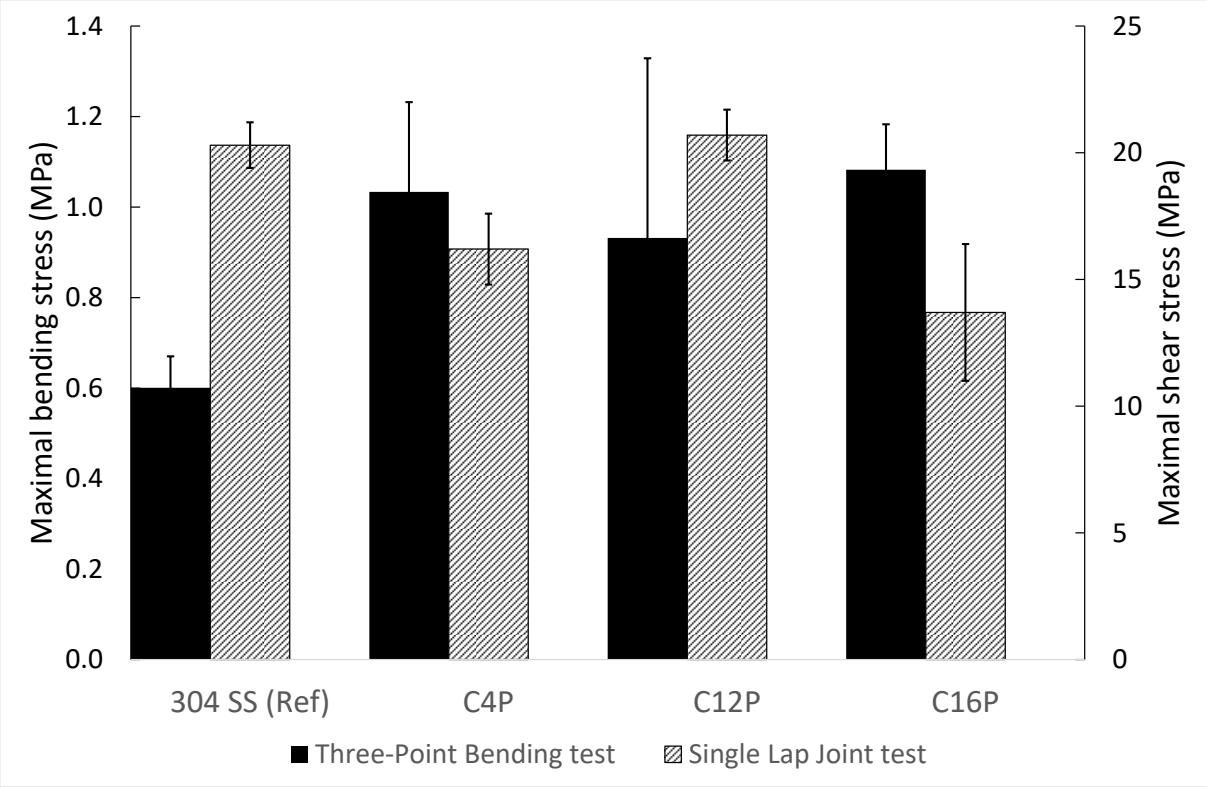

Figure 4: Effect of carbon chain length in Single Lap Joint (in right with patterns) and Three-Point Bonding tests (in left in black)

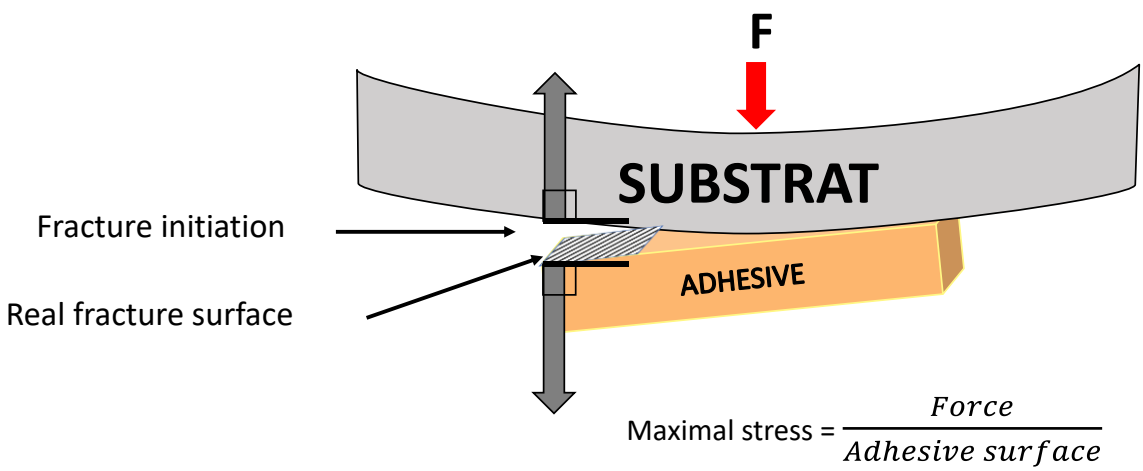

Figure 5: Schematic illustration of fracture initiation in a three-point bending test

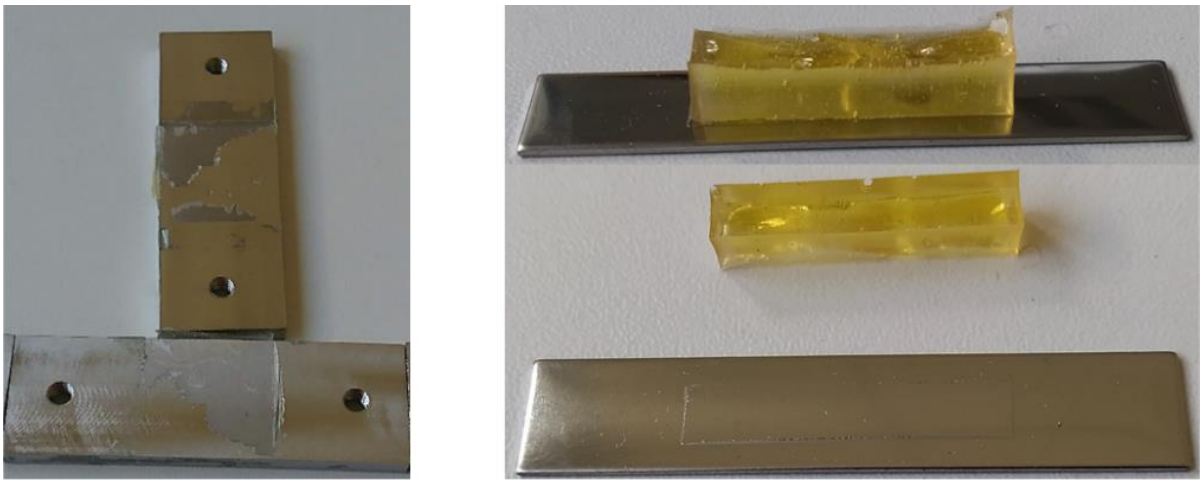

Figure 6: Single Lap joint (left) and three-point bending (right) samples

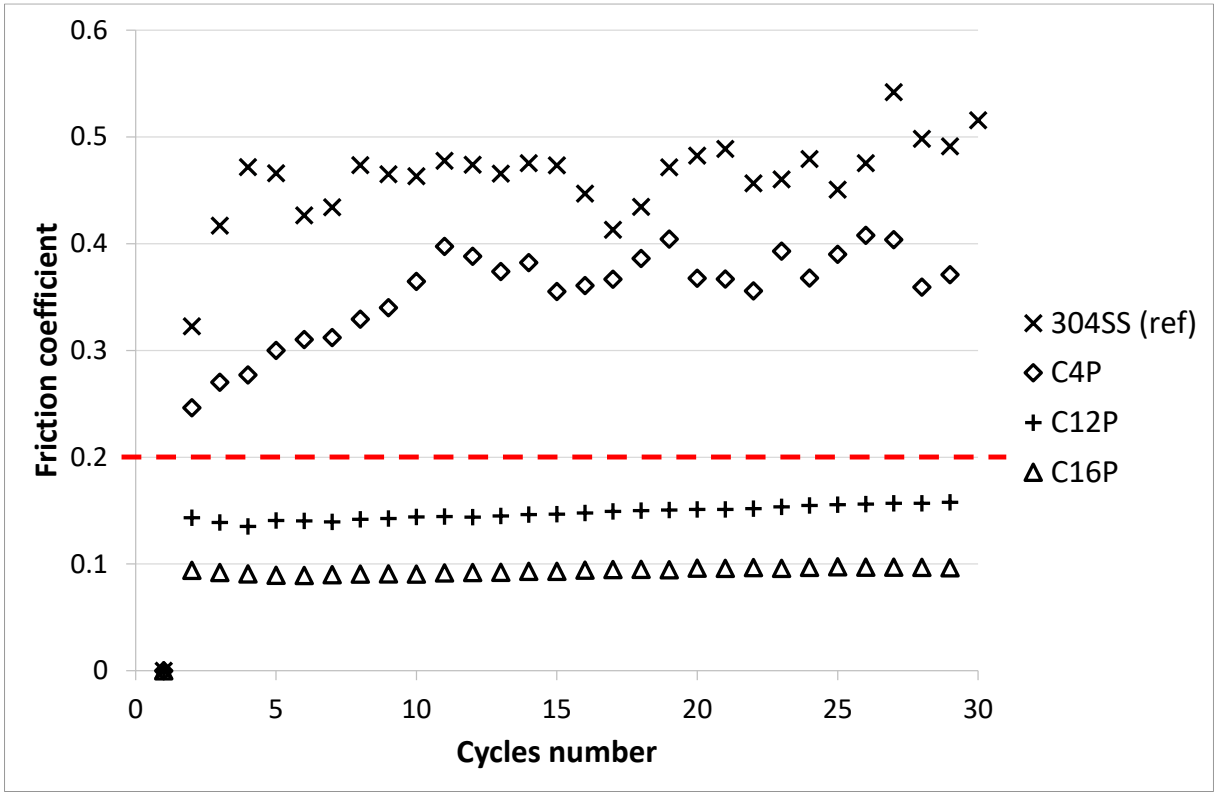

Figure 7: Friction coefficient of SAMs samples after Three Point Bending tests

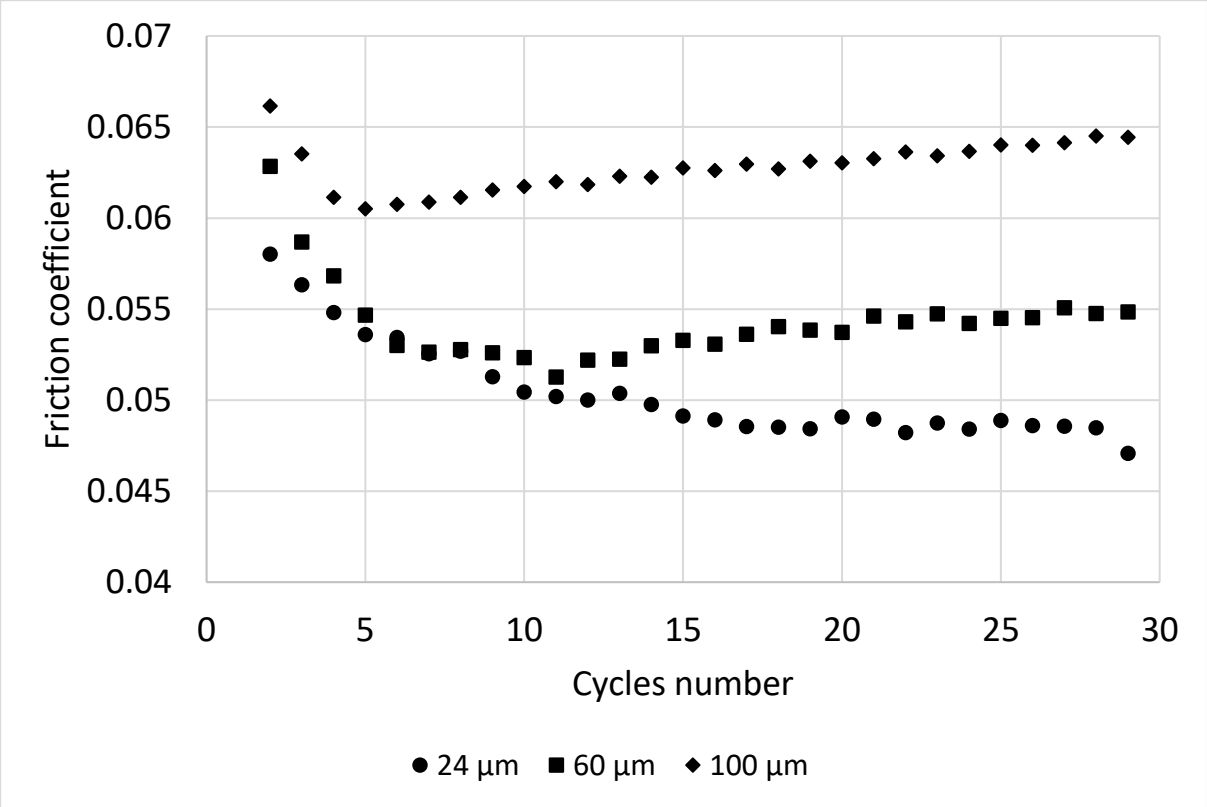

Figure 8: Friction coefficient as a function of Araldite film thickness

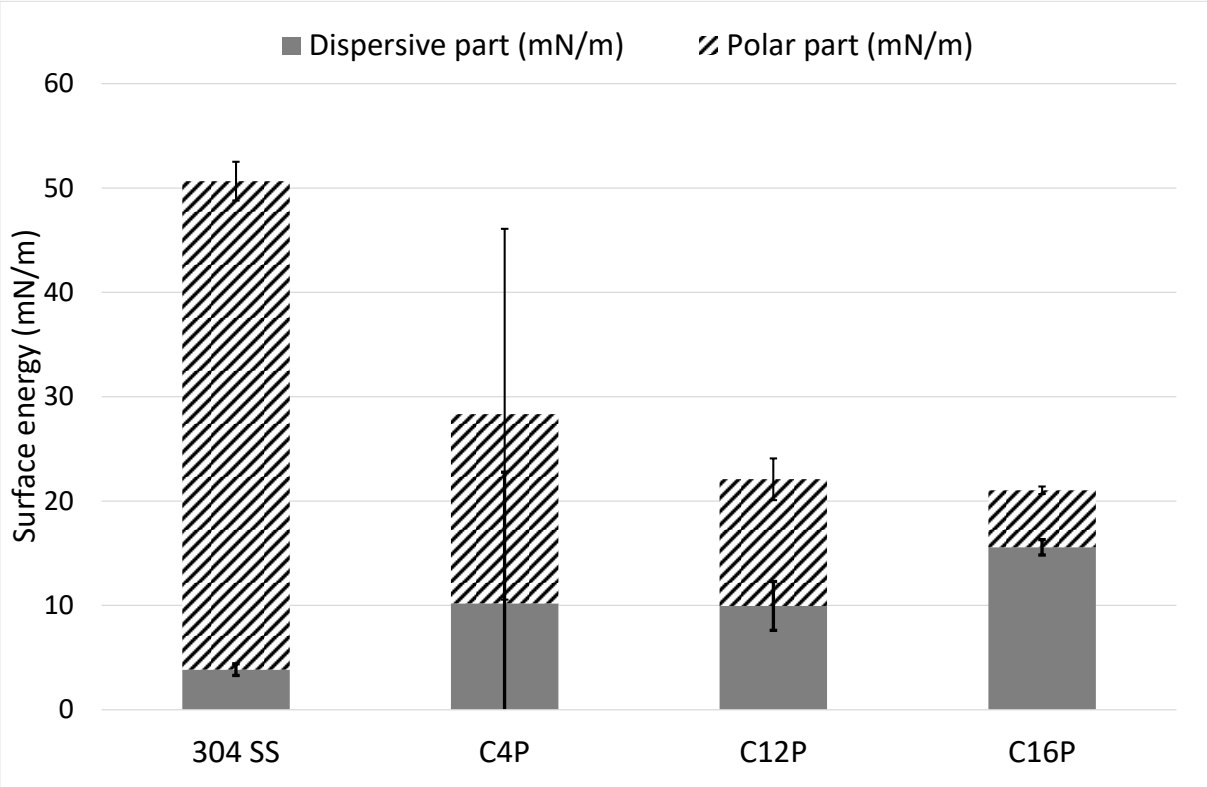

Figure 9: Surface energy characterization for various length carbon chain

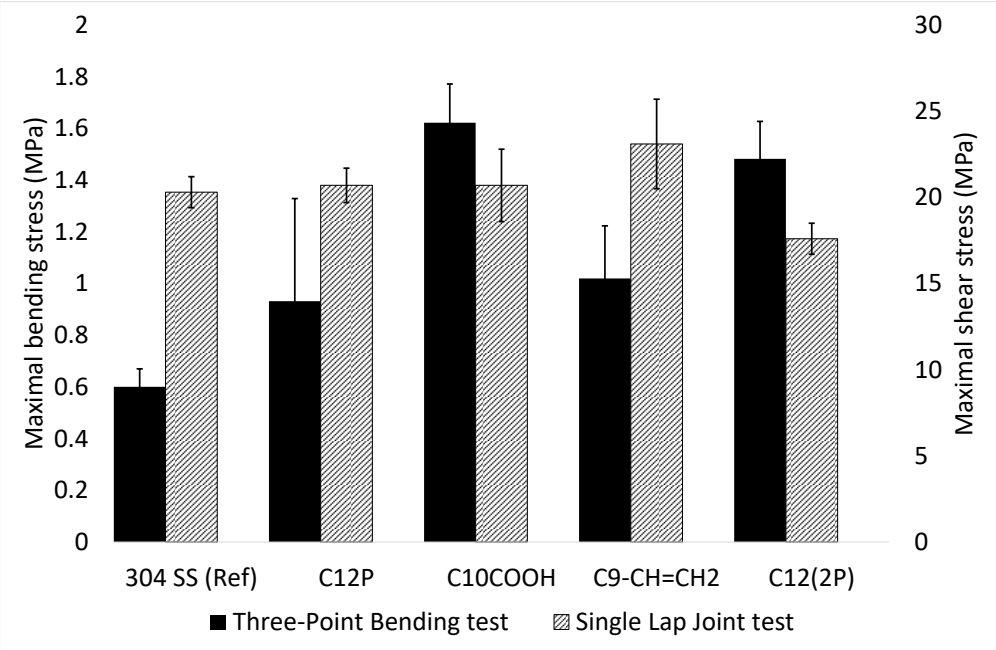

Figure 10: Effect of terminal group in Single Lap Joint (in right with patterns) and three-point bending tests (in left in black)

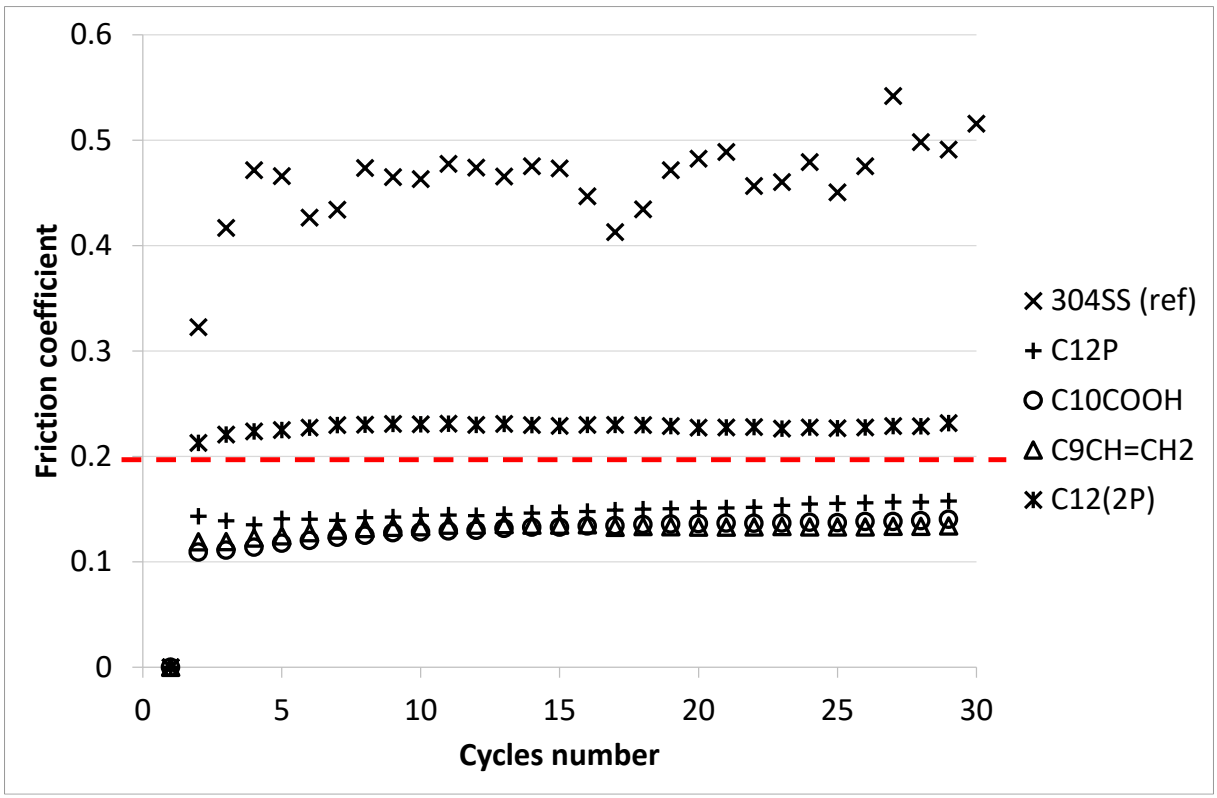

Figure 11: Friction coefficient of SAMs samples after three-point bending test

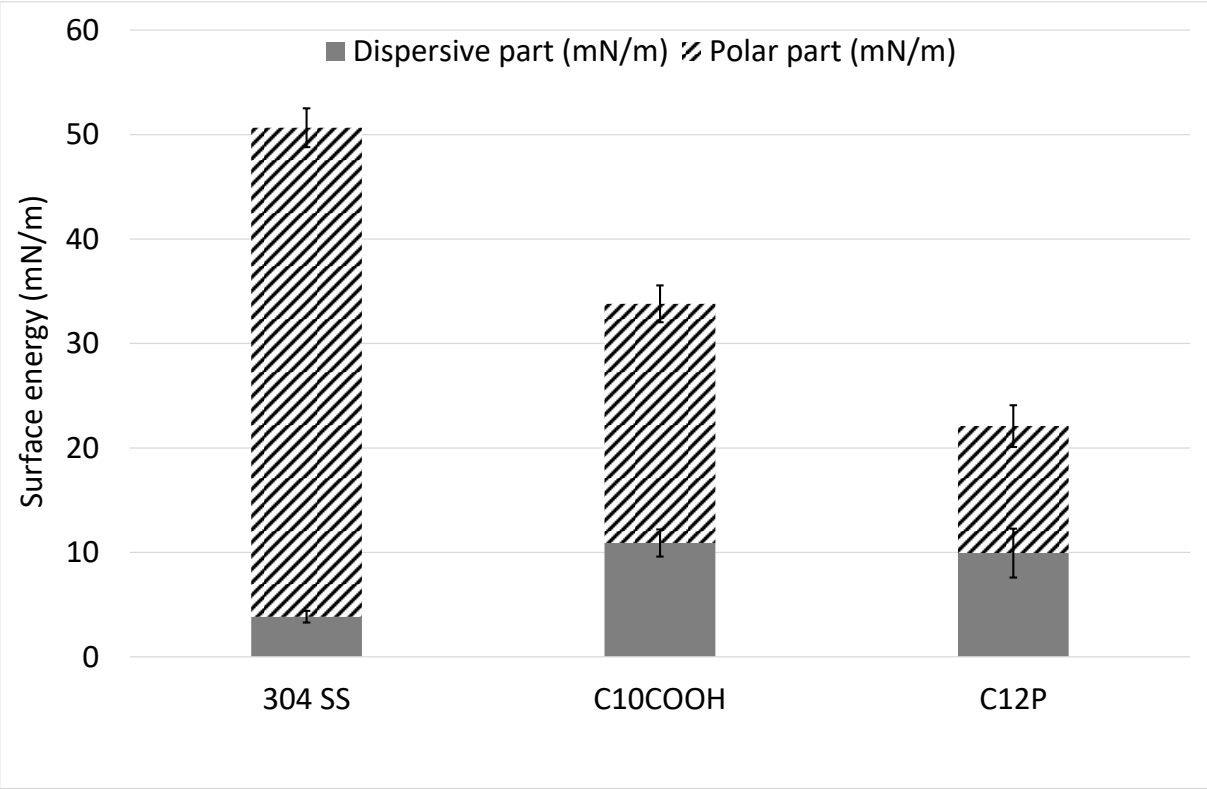

Figure 12: Surface energy characterization for two terminal groups

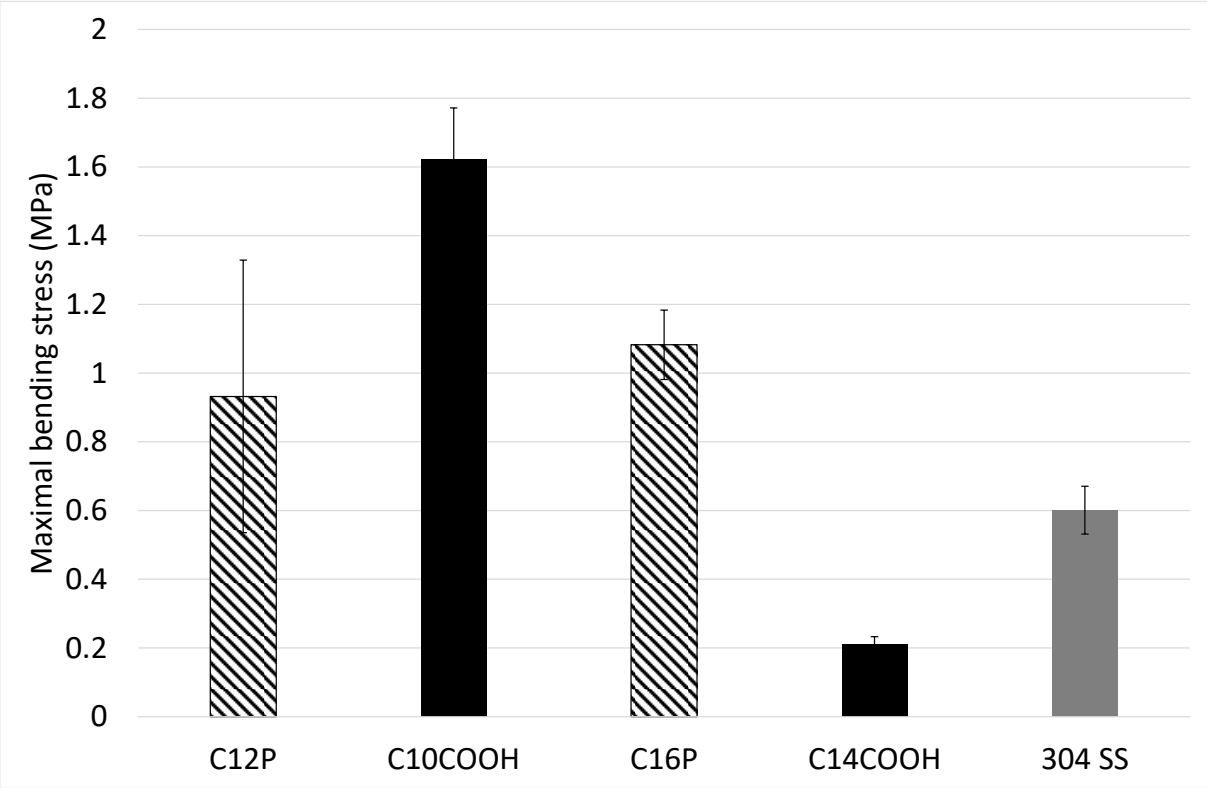

Figure 13: Effect of terminal group with longer carbon chain in three point Bending test, the apolar (alkyl) terminations are shown in patterns and the polar (carboxyl) terminations are represented in black

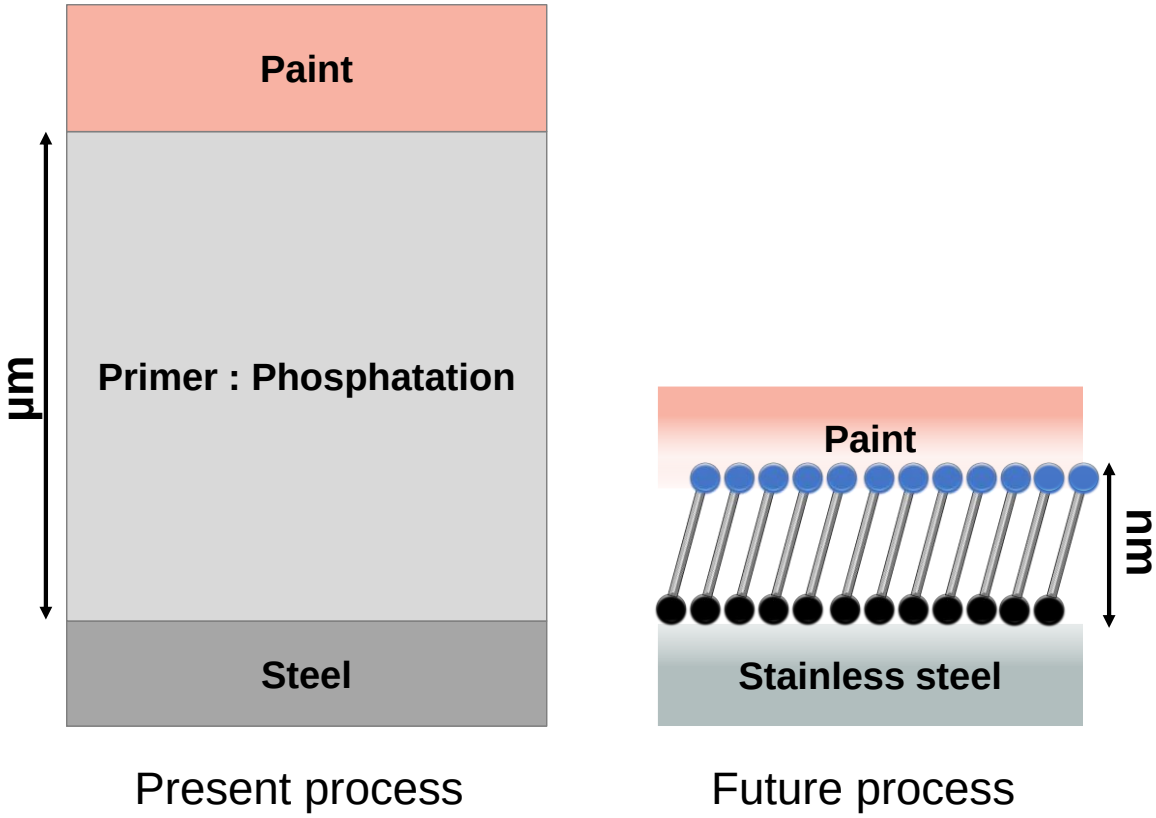

Figure 14: Schematic representation of the two study systems

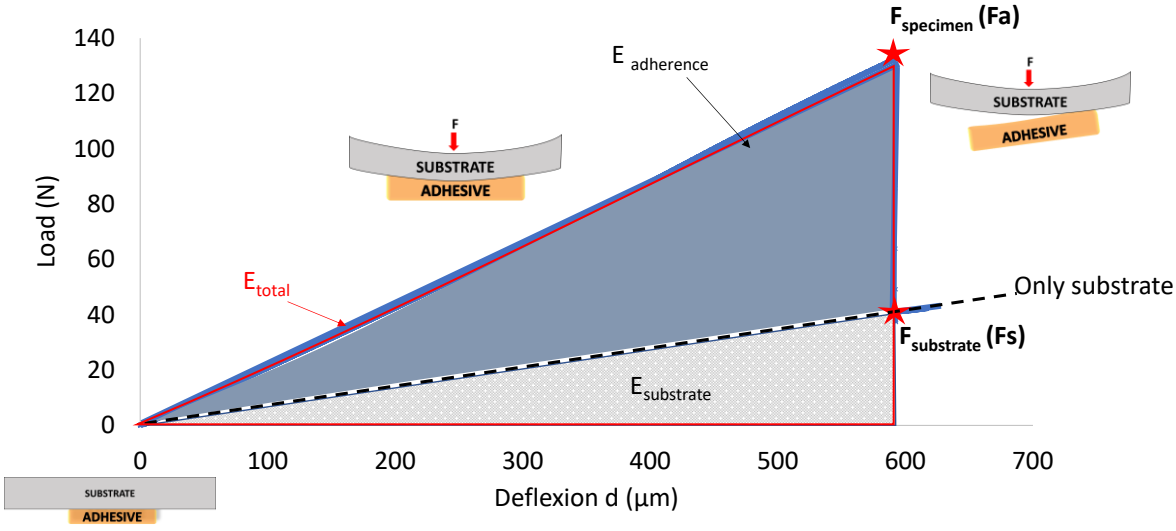

Figure 15: A typical adherence curve in three-point bending

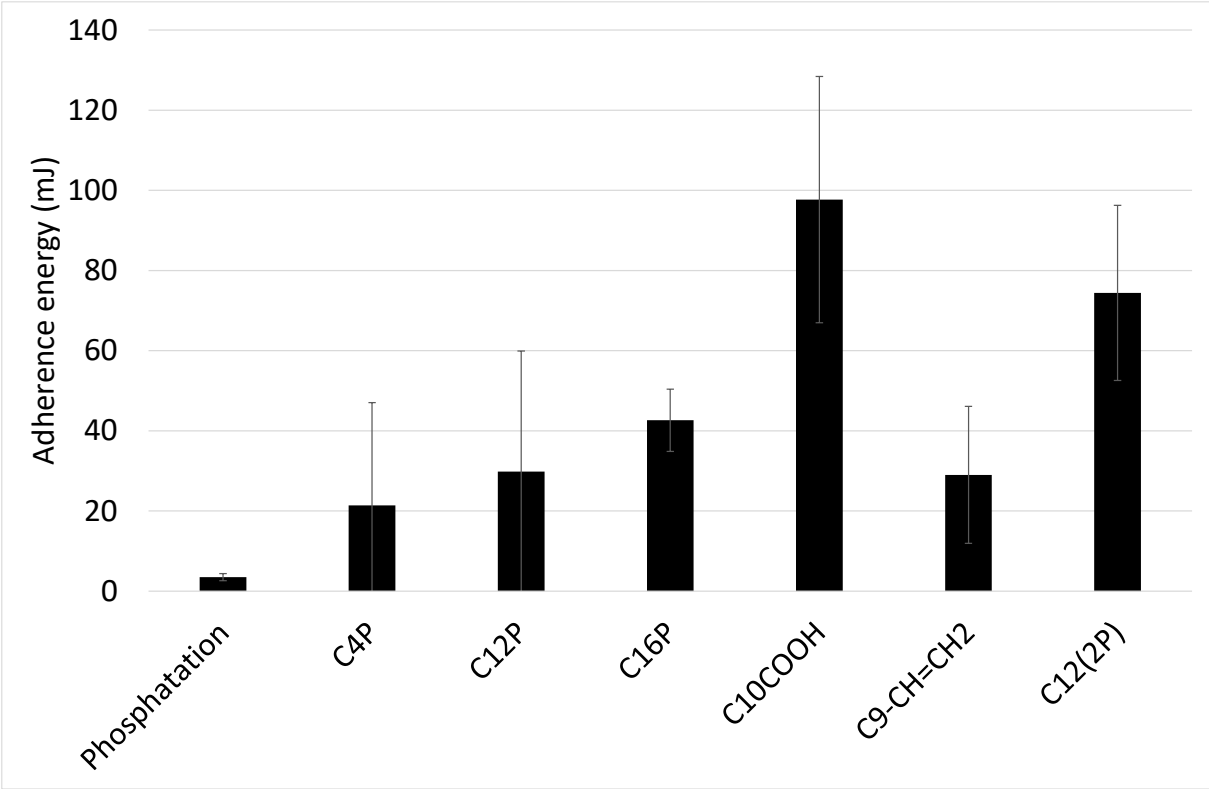

Figure 16: Adherence energy in three-point bending test

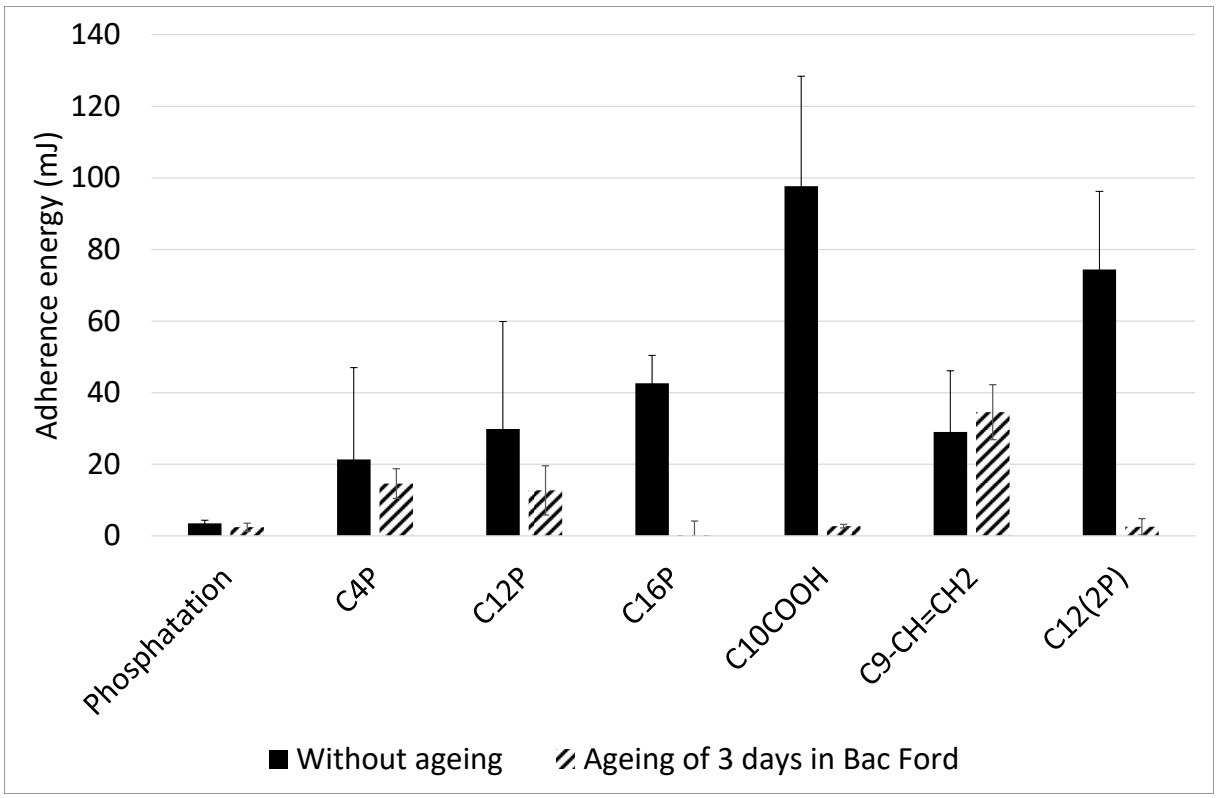

Figure 17: Impact of ageing in Bac Ford test

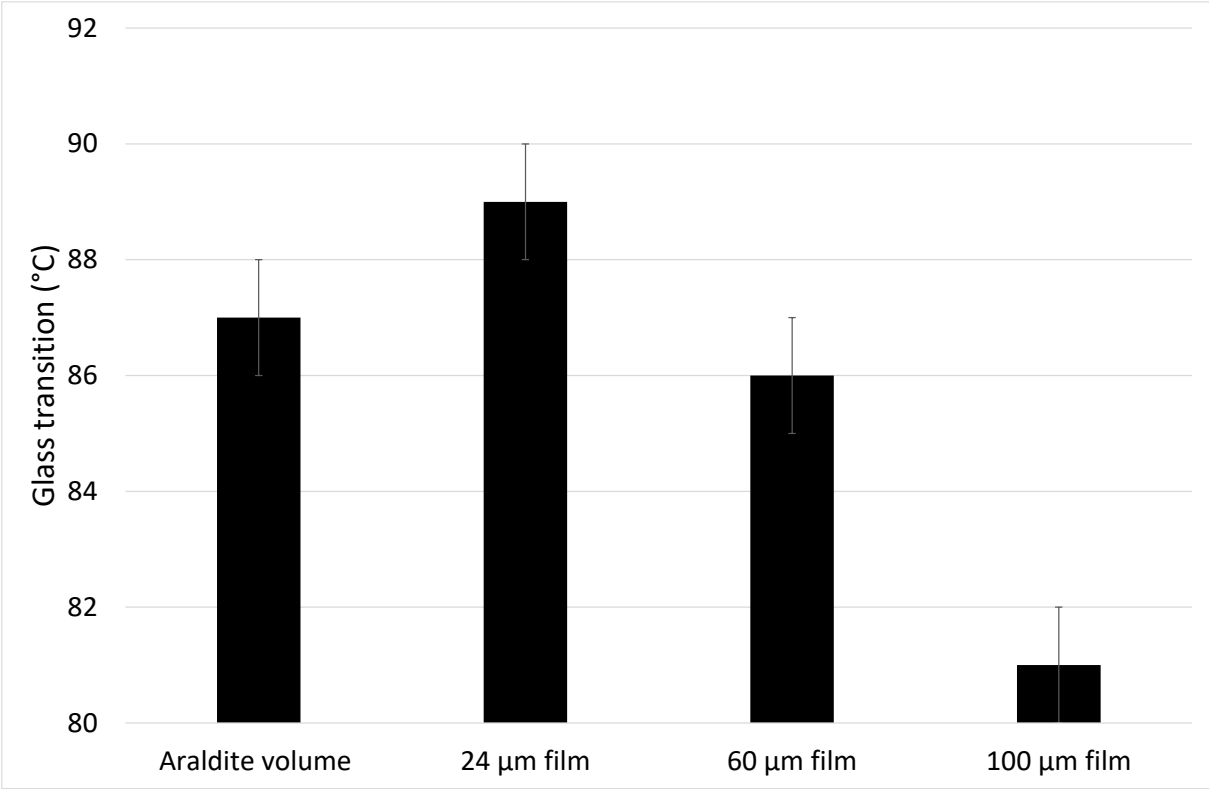

Figure 18: Evolution of the glass transition temperature (onset values) as a function of the glue thickness on 304SS substrate

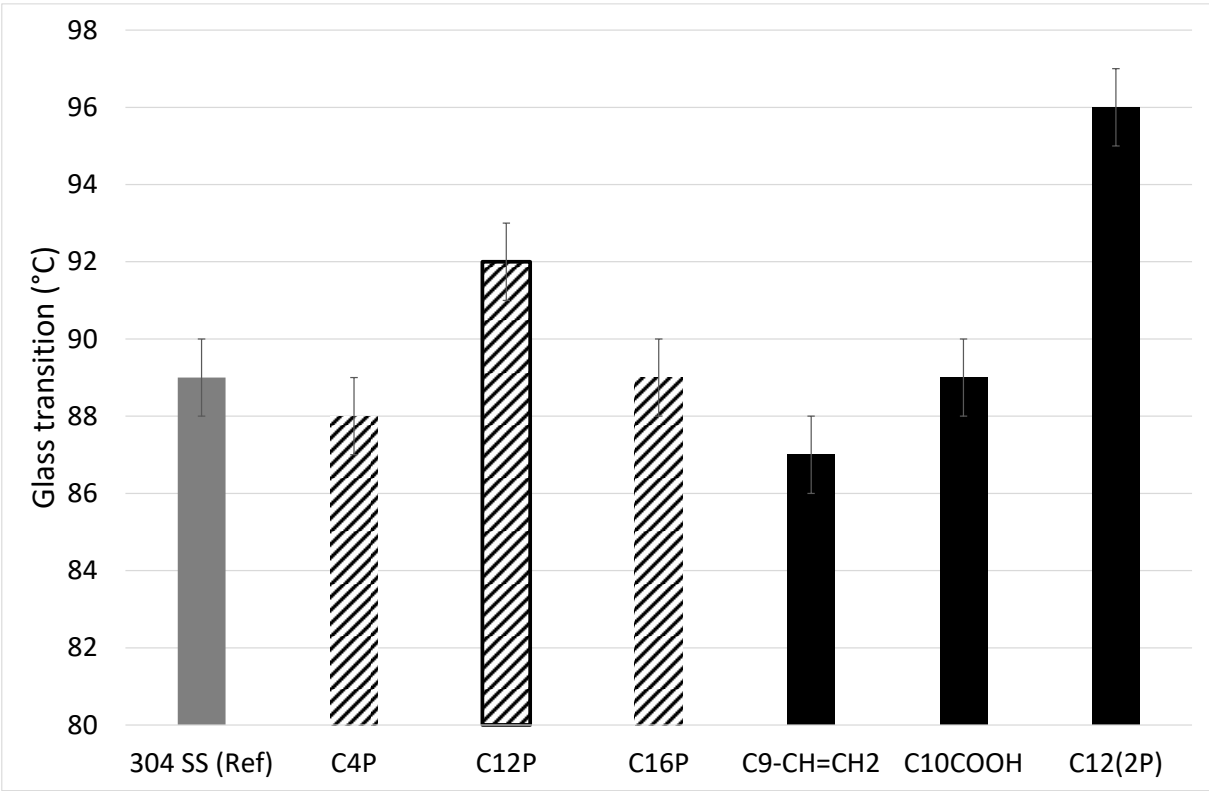

Figure 19: Glass transition according to the tested interphases. The variation of the length of the carbon chain is shown in patterns and the variation of the terminal groups in black. In grey, it’s the reference without treatment.